NUREG/CR-0686
(ORNL/NUREG/TM-309)

cy.29

Advanced Two-Phase Flow Instrumentation Program Quarterly Progress Report for July-September 1978

K. G. Turnage
C. E. Davis
D. G. Thomas

Prepared for the U.S. Nuclear Regulatory Commission
Office of Nuclear Regulatory Research
Under Interagency Agreements DOE 40-551-75 and 40-552-75

OAK RIDGE NATIONAL LABORATORY
OPERATED BY UNION CARBIDE CORPORATION · FOR THE DEPARTMENT OF ENERGY

Printed in the United States of America. Available from
National Technical Information Service
U.S. Department of Commerce
5285 Port Royal Road, Springfield, Virginia 22161

NUREG/CR-0686
ORNL/NUREG/TM-309
Dist. Category R2

Contract No. W-7405-eng-26

Engineering Technology Division

ADVANCED TWO-PHASE FLOW INSTRUMENTATION PROGRAM QUARTERLY PROGRESS REPORT FOR JULY-SEPTEMBER 1978

K. G. Turnage
C. E. Davis D. G. Thomas

Manuscript Completed — April 17, 1979
Date Published — May 1979

Prepared for the
U.S. Nuclear Regulatory Commission
Office of Nuclear Regulatory Research
Under Interagency Agreements DOE 40-551-75 and 40-552-75

NRC FIN No. B0401

Prepared by the
OAK RIDGE NATIONAL LABORATORY
Oak Ridge, Tennessee 37830
operated by
UNION CARBIDE CORPORATION
for the
DEPARTMENT OF ENERGY

CONTENTS

ADVANCED TWO-PHASE FLOW INSTRUMENTATION PROGRAM QUARTERLY PROGRESS REPORT FOR JULY-SEPTEMBER 1978

K. G. Turnage
C. E. Davis D. G. Thomas

ABSTRACT

A series of two-phase air-water tests with advanced spool piece I in horizontal flow is described. Nine drag body designs were tested to evaluate their suitability for two-phase momentum flux measurements by comparing drag flowmeter output with three independently calculated quantities. Preliminary analysis indicates that, in terms of drag flowmeter agreement with other estimates of the two-phase momentum flux, the blade-type targets and two perforated plate designs performed better than the other types. Analysis of data from the densitometer, turbine meter, and pressure-difference cell in the spool piece is also presented. Application of some two-phase mass flow models to the recorded data is discussed, and preliminary results are shown.

1. INTRODUCTION

The measurement of two-phase mass flow rate is of primary importance in experimental programs involving loss-of-coolant studies. Because of the severe environments present during blowdown, relatively few instrument types have gained widespread acceptance; these include turbine meters, gamma densitometers, and drag flowmeters. (Pressure and temperature measurements are also required for reduction of data from the other instruments.)

When two-phase mass flow rate measurements are desired, full-flow instruments have often been located in a relatively short piping segment called a spool piece. The design of spool pieces is important because the turbine meter and drag flowmeter are intrusive and may seriously alter the flow regime. Conversely, location of all three instruments in close proximity is desirable because of the often unsteady and inhomogeneous nature of two-phase flow.

The advanced spool piece being used in the current studies[1] is shown in Fig. 1.1. Unique attributes include allowance for two drag

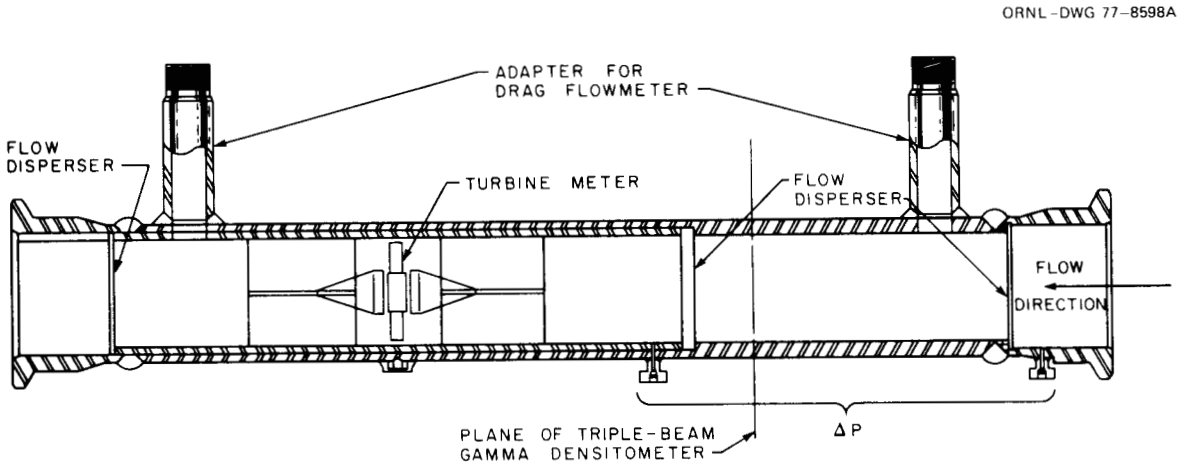

Fig. 1.1. Advanced spool piece I.

body flowmeters and three flow-dispersing screens. The drag transducers used are like those in use for some time at Oak Ridge National Laboratory (ORNL), but several additional experimental drag targets have been tested. Also, a three-beam gamma densitometer and a full-flow turbine meter are being used. When flow-dispersing screens are in the spool piece, pressure difference measurements may be used as an indication of the two-phase momentum flux.

During the current quarter, a series of horizontal flow experiments with advanced spool piece I in the ORNL Air-Water Test Facility was completed. The tests included use of nine experimental drag targets, with the drag flowmeter lever arm penetrating the spool piece from the top. Runs have also been made using various drag targets having the spool piece oriented so that the lever arms entered the pipe horizontally and from the bottom. The effects of flow-dispersing screens on the instrument behavior were also investigated.

Analysis of data from these tests has included review of the individual instrument response and use of several two-phase mass flow models that use input from two or more instruments. Comparisons between stratified and annular models for reduction of three-beam densitometer data have been made. The Aya, Rouhani, and volumetric turbine meter models have been used, with mean phase velocity data for comparison with mean velocities based on turbine meter readings. Extensive analysis of

drag target behavior is being performed. Finally, pressure-difference measurements across flow-dispersing screens are being used in mass flow models and compared to estimated values of the momentum flux. Studies of two-phase mass flow models have involved estimating the errors resulting from applying homogeneous models to postulated two-velocity systems. Difficulties in application of the Aya model to two-phase air-water data have required use of additional assumptions, with model failure still occurring at some flow rates.

2. FACILITY DESCRIPTION

The ORNL two-phase air-water loop (Fig. 2.1) is capable of supplying air at flow rates up to 242 liters/sec (512 scfm) and water at flow rates up to 32 liters/sec (500 gpm). In the 8.9-cm-ID (3.5-in.) spool piece tested, those rates correspond to superficial velocities of 39 m/sec (128 fps) for air and 5.2 m/sec (17 fps) for water. (When elements of large hydraulic resistance are in the loop, the highest two-phase flow rates are often not obtainable.) For this study, 4.6 m (15 ft) of straight, clear 4-in. polyvinyl chloride (PVC) piping (10.2 cm ID) was located upstream of the stainless steel test section and 1.2 m (4 ft) was located downstream. The two-phase air and water flows were at ambient temperature and near atmospheric pressure.

In the air-water loop, air flow rate is determined using a pressure gauge upstream of the critical flow orifices, and water is metered into

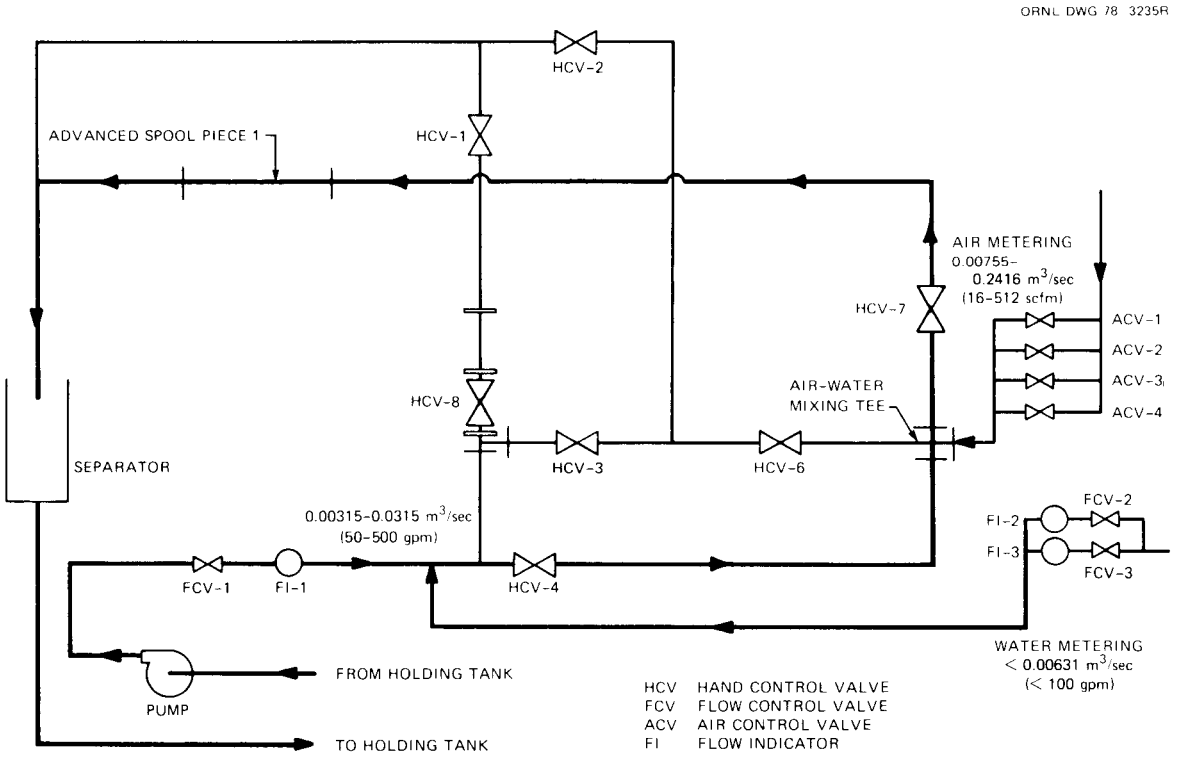

Fig. 2.1. Location of advanced spool piece I in ORNL two-phase air-water loop during horizontal flow tests. Heavy line indicates flow path for current tests.

the loop by means of rotameters [flow rates <6.3 liters/sec (100 gpm)] or a magnetic flowmeter. No special measures were taken to enhance mixing; however, the observed flow regimes in the horizontal section were in good agreement with the flow regime map of Mandhane et al.[2] (Fig. 2.2).

The experiment was conducted by setting the desired air flow rate and then taking data at successively higher water input rates until either the system pressure became high enough to unchoke the critical flow orifice or one of the instruments was overranged. The air flow rate was then doubled, and the procedure of taking data with various water flow rates was repeated.

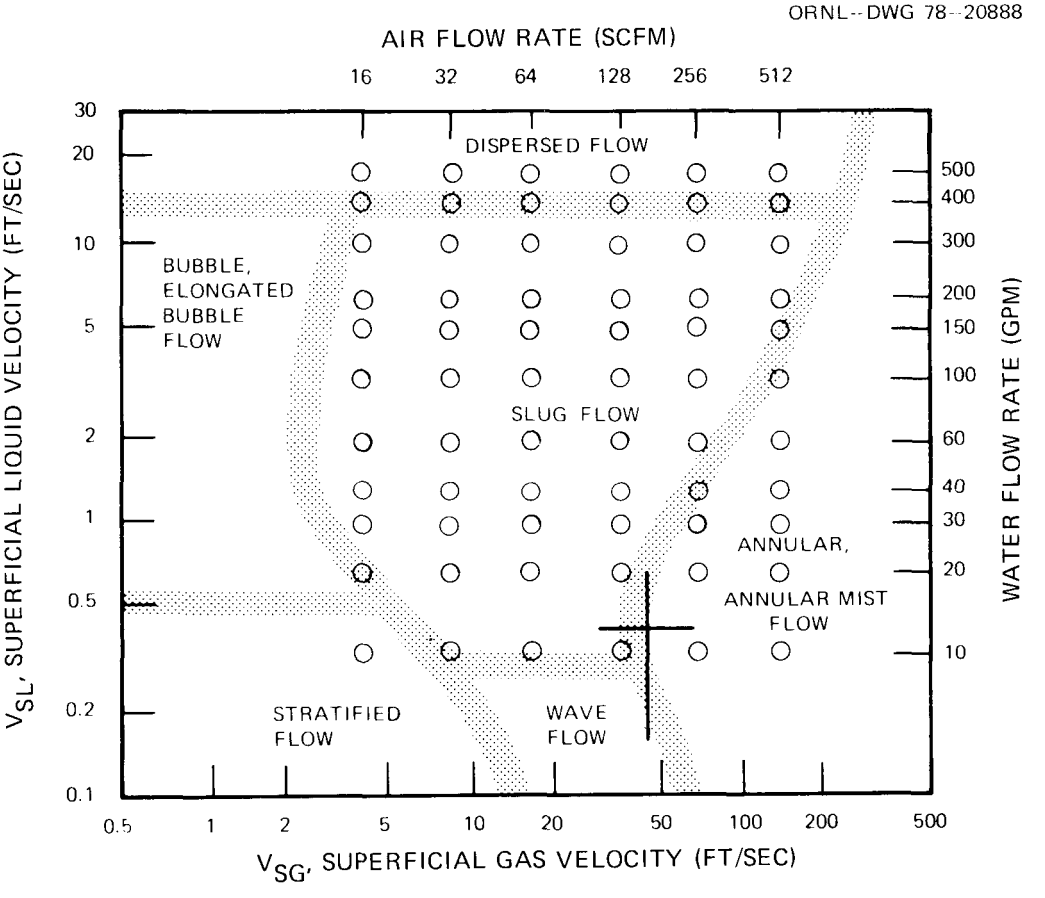

Fig. 2.2. Flow pattern map proposed by Mandhane et al.[2] Circles are points at which data were taken during current tests.

3. NEW DATA REDUCTION METHODS

The electronics, data acquisition system, and basic data reduction techniques used for air-water studies are described in the previous quarterly report.[3] An improvement made in the method of reduction of experimental data is described.

Measurements of two-phase flow parameters are often most difficult for the least steady flow regimes (e.g., slug flow). Even when metered single-phase input flow rates are essentially constant, the resulting two-phase flows at the measurement locations may oscillate widely in velocity, density, and mass flux. In fact, accurate measurement under those conditions is, in some ways, similar to the problem of transient mass flux measurements during blowdown, when rapid changes in local flow patterns also occur.[4]

Calculations of two-phase flow parameters which involve input from two or more instruments over a scan time (data-taking period) may be made in one of two ways: (1) each instrument output may be averaged over the scan and the final results put into the model equations, or (2) the model equations may be evaluated using instantaneous or short time averages from the instruments; the results from many evaluations of the model equations may then be averaged over the scan. For example, if a quantity X was to be modeled as product of two instrument outputs r(t) and s(t), method 1 would give

$$X_1 = \left[\frac{1}{T}\int_o^T r(t)\ dt\right]\left[\frac{1}{T}\int_o^T s(t)\ dt\right] , \tag{3.1}$$

and method 2 would give

$$X_2 = \frac{1}{T}\int_o^T r(t)\ s(t)\ dt . \tag{3.2}$$

Clearly, $X_1 \neq X_2$ for most nonconstant functions r and s.

Analysis codes used to calculate transient mass fluxes from instrument responses use instantaneous or short time averages ($\lesssim$0.1 sec) of

voltage readings as inputs to the mass flux models. The evaluation of measurement systems intended for transient applications in steady-state facilities should, therefore, use method 2 for data reduction.

The data reduction code described previously[3] has been modified to perform calculation of all models using method 2. A comparison of results for the ratio $G_2 = (\overline{\rho I_d})^{1/2}/G_{actual}$ using the two methods may be made using Fig. 3.1. For this typical example, significant differences occurred only for flow rates with low air and water input. In practice, most instrument outputs may be approximated as a constant term plus a periodically varying term. At moderate and high flow rates, the constant term is fairly large compared with the varying term, and $X_1 \approx X_2$.

At low flow rates, when slugging occurs, the majority of the signal output from a turbine or drag flowmeter may arise from passage of a few large slugs. Then, significant differences between the two methods may occur. If the instrument separation is large and the slug velocity is relatively low, the slug may reach the two instruments at distinctly different times. In such cases, the value of X_2 would be lower than it should be, and X_2 would underestimate the correct value of X, even if X_2 were a perfect model. For the same conditions, calculation of X using method 1 would also be improper.

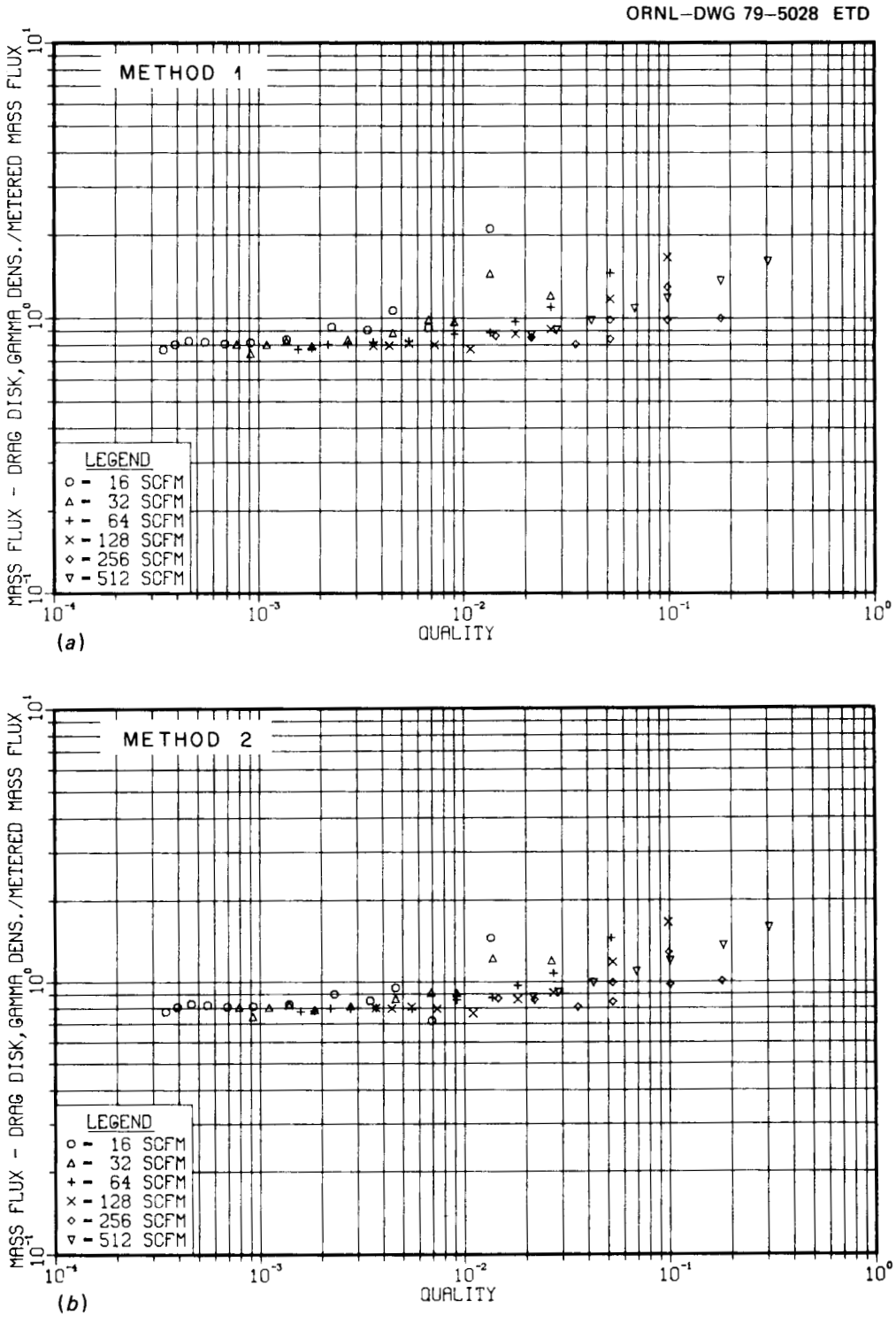

Fig. 3.1. Ratio of mass flux calculated from drag flowmeter and densitometer data to actual mass flux: method 1 (a) and method 2 (b).

4. INDIVIDUAL INSTRUMENT RESPONSE

4.1 Three-Beam Densitometer

4.1.1 Densitometer models

The model used for calculating the two-phase density from the three-beam gamma densitometer assumes annular flow through the test section. In horizontal flow, the annular flow regime is not the most predominant regime, but the annular density model was found to yield essentially the same results as a stratified model when it was applied to the same densitometer data.

A stratified model for calculating density has been developed at ORNL and is an "area weighted" model, with each densitometer beam sampling only one region of the pipe cross-sectional area (Fig. 4.1); the annular model[3] allows the three beams to sample one or more of the three concentric regions. Because each beam will sample only one region for the stratified model, the ratio of the area sampled by the beam to the total area of the pipe is the weighting factor used to calculate the total composite density from the individual beam density. The densitometer configuration at the ORNL air-water loop produces an A-beam sampling area of 21.7 cm^2 (3.309 $in.^2$), a B-beam area of 30.2 cm^2 (4.678 $in.^2$), and a C-beam area of 10.2 cm^2 (1.574 $in.^2$). Thus the composite density using the stratified flow model can be calculated by

$$\bar{\rho}_{st} = 0.3502\ \rho_A + 0.4862\ \rho_B + 0.1636\ \rho_C\ , \tag{4.1}$$

and the annular model density[3] is equal to

$$\bar{\rho}_{an} = 0.3784\ \rho_A + 0.5117\ \rho_B + 0.1099\ \rho_C\ . \tag{4.2}$$

In horizontal two-phase flow, ρ_A and ρ_B are generally higher than ρ_C. Because ρ_A and ρ_B are more heavily weighted and ρ_C is less heavily weighted in the annular model, that model calculates a higher density than the stratified model at some qualities. However, the average

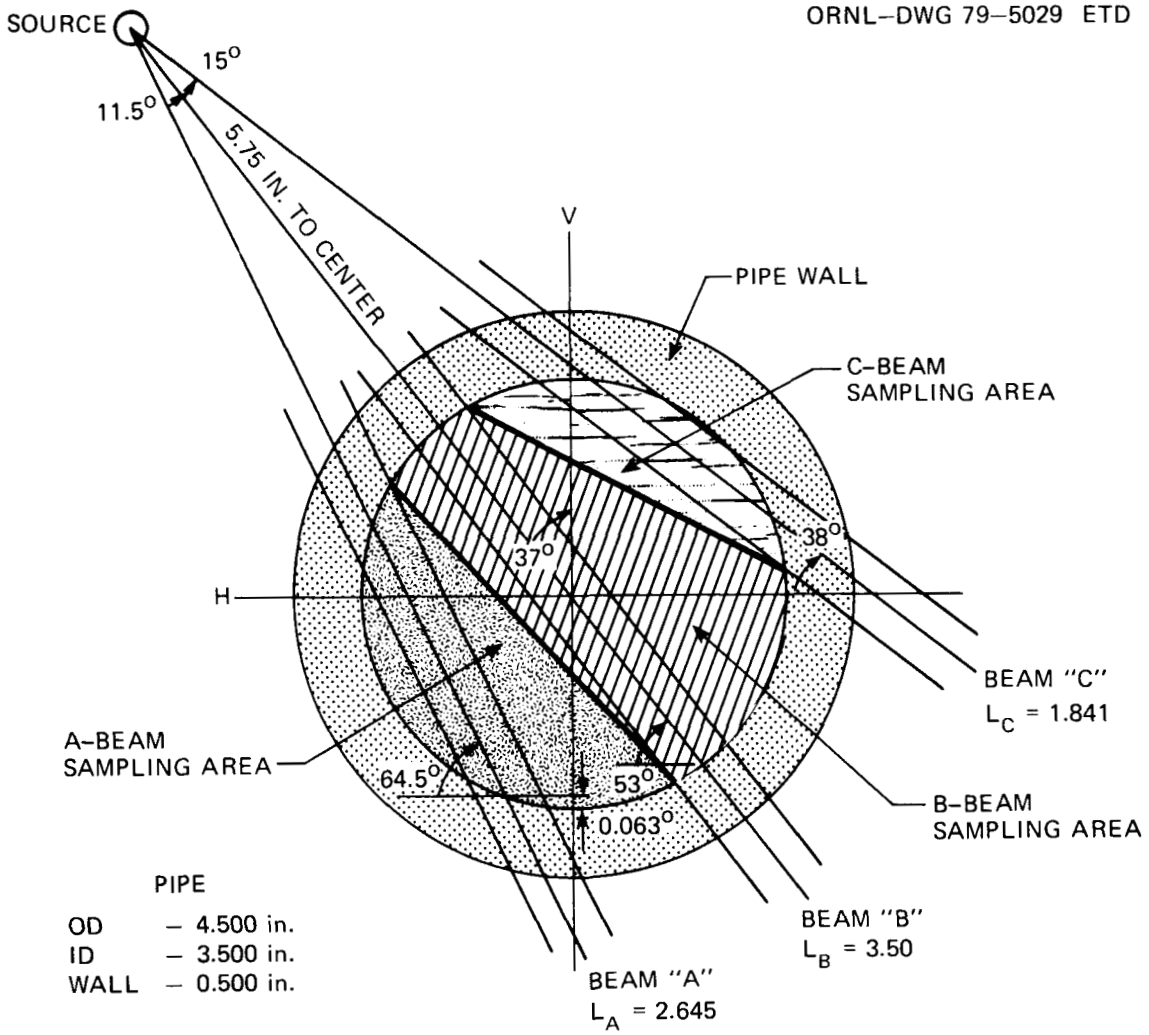

Fig. 4.1. Each beam of the three-beam gamma densitometer samples its own individual area for the stratified model calculations.

difference between the annular and stratified models is only ∿5% (Fig. 4.2). The greatest difference usually occurs at a quality of ∿1%, but even the largest difference there is normally ∿10%.

In advanced spool piece I, the upstream drag flowmeter plays an important role in causing the annular model calculation of the two-phase density to be similar to the stratified model. Visual observations using a transparent spool piece reveal some interesting behavior of the two-phase mixture as it passes the full-flow drag target. Figure 4.3 shows that, when the flow upstream of the target is definitely stratified,

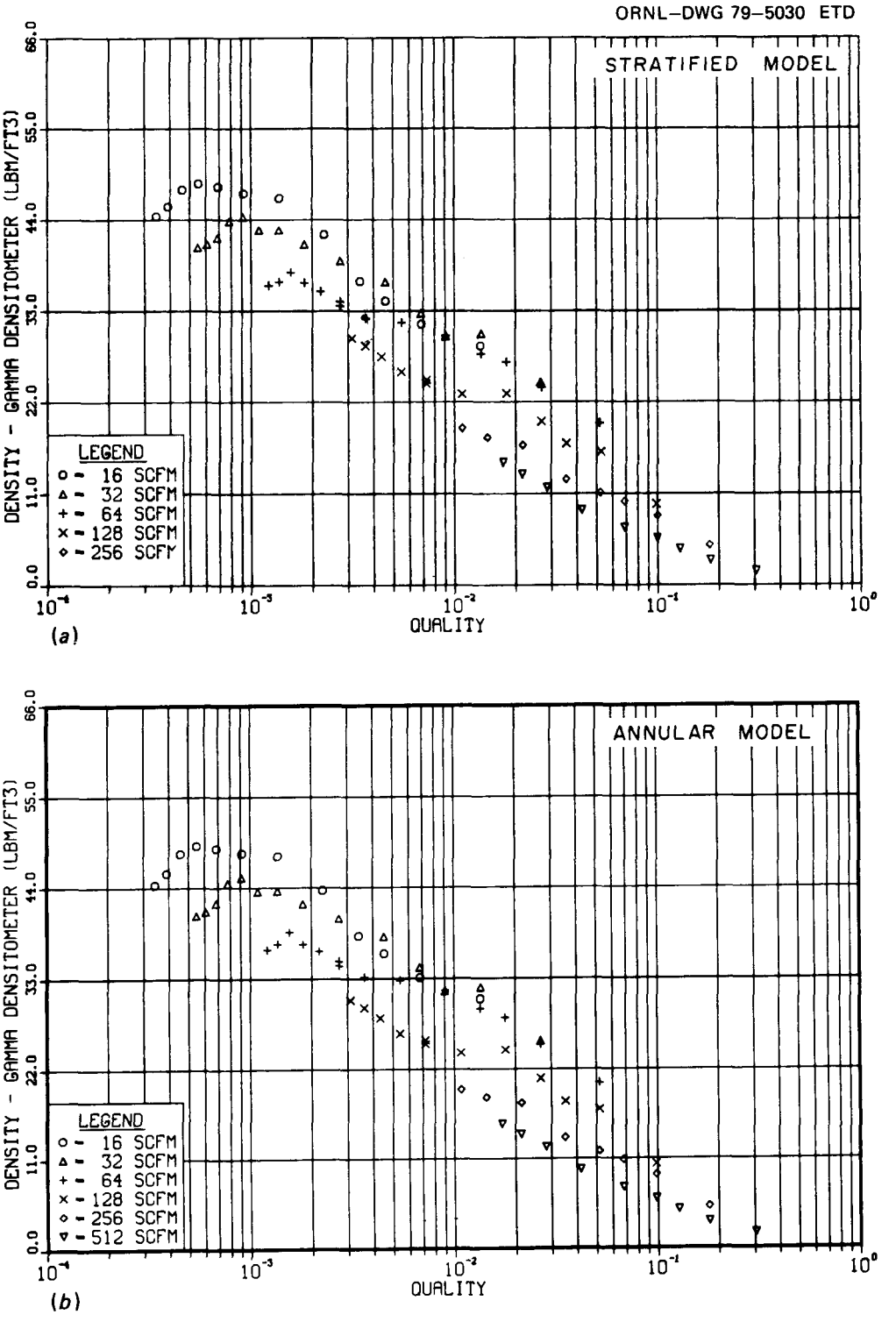

Fig. 4.2. Little difference exists between the densities calculated from three-beam densitometer data using the stratified model (a) and the annular model (b). A 2.54-cm (1-in.) disk drag target was upstream of the densitometer.

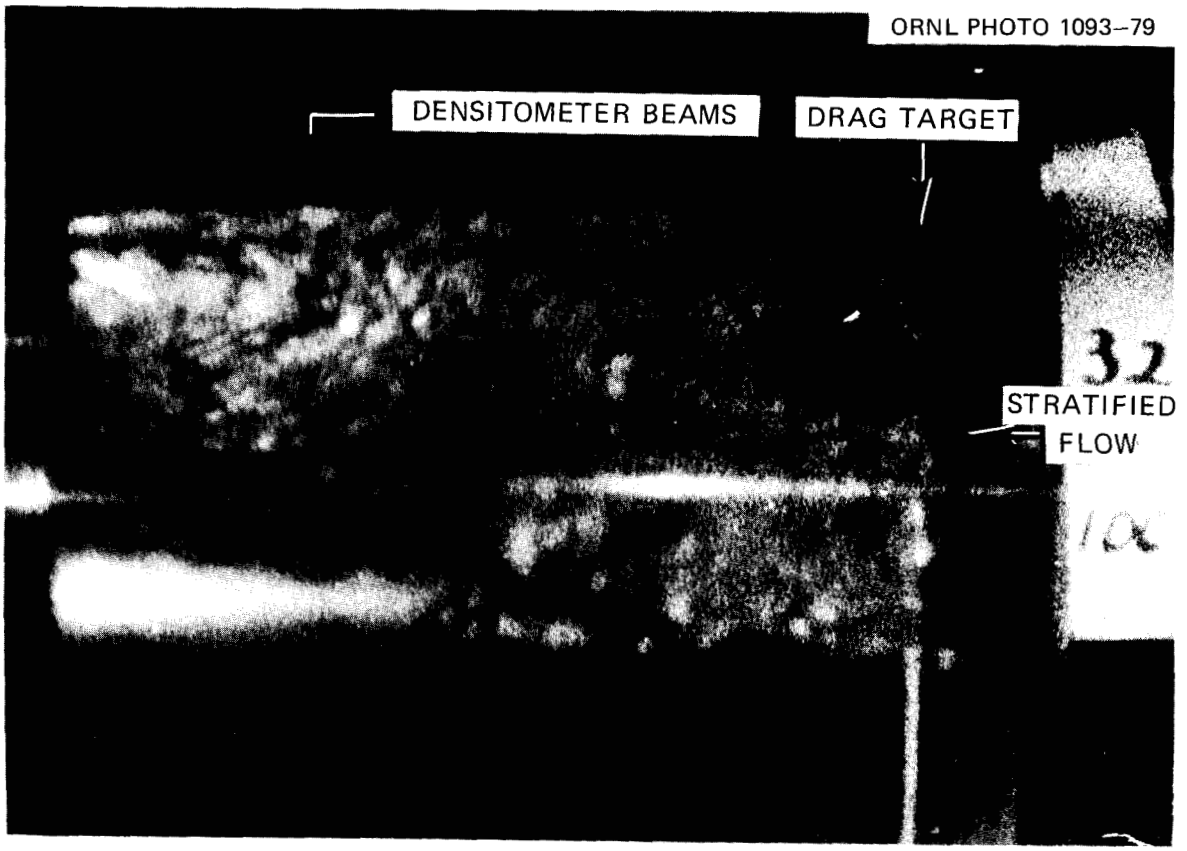

Fig. 4.3. At 15.1 liters/sec (32 scfm) and 6.3 liters/sec (100 gpm), the flow upstream of the perforated plate drag target is definitely stratified; however, the flow is apparently annular downstream of the target.

the full-flow drag target (a perforated plate in this case) disperses the liquid to the walls of the pipe. This film of water on the top and side walls of the test section near the location of the densitometer beams was noticed nearly every time stratified flow occurred before the drag target and resulted in the annular model being a suitable calculation for the two-phase density.

4.1.2 Effect of the drag target wake on the densitometer

The calculated density from the three-beam gamma densitometer is often compared to the homogeneous density based on the metered flow rates of each phase. Composite density from densitometer data is normally higher than the homogeneous density, which indicates that the

slip ratio is greater than unity in horizontal flow. However, there is a peculiar density decrease that occurs at very low qualities (Fig. 4.4). This is probably due to a perturbation in the flow regime at the plane of the densitometer caused by the drag target and its adapter. Figure 4.4 shows data from an experiment where the spool piece has been rotated 180° about its axis so that the drag target adapters are on the bottom of the test section. With the 1.3-cm (0.5-in.) drag target, a dramatic change in this rolling characteristic is apparent, only because of the orientation change of the adapters for the drag targets. The same comparison is made in Fig. 4.5 for the three-bladed drag target. A slight reduction in the low-quality rolloff is present, but the change is not as substantial as with the 1.3-cm (0.5-in.) disk. This change in the density rolloff with the three-bladed target is expected to be small for each 90° spool piece rotation about its axis because the geometric symmetry of the target orientation varies little with the rotation.

The drag target and its orientation obviously have an effect on the densitometer readings in some quality ranges. The experimental data suggest that the adapter cavity or the arm of the drag flowmeter may be the major source of this behavior. This low-quality rolloff of the composite density also could possibly be related to the flow regime change that occurs near the superficial liquid and gas velocities for these qualities. This density rolling characteristic occurs at air flow rates of 7.55, 15.1, and 30 liters/sec (16, 32, and 64 scfm) and water flow rates of 19 and 25.2 liters/sec (300 and 400 gpm), which is near the flow regime change from a slug flow to dispersed flow according to the horizontal flow regime map proposed by Mandhane[2] (Fig. 2.2).

4.2 Turbine Meter

4.2.1 Turbine electronics

The Instrumentation and Controls Division of ORNL has developed a set of electronics to interpret the turbine meter pickoff output. These new electronics make the turbine meter readings more responsive to changes in the turbine rotation speed and also are capable of detecting lower flow rates in the pipe.

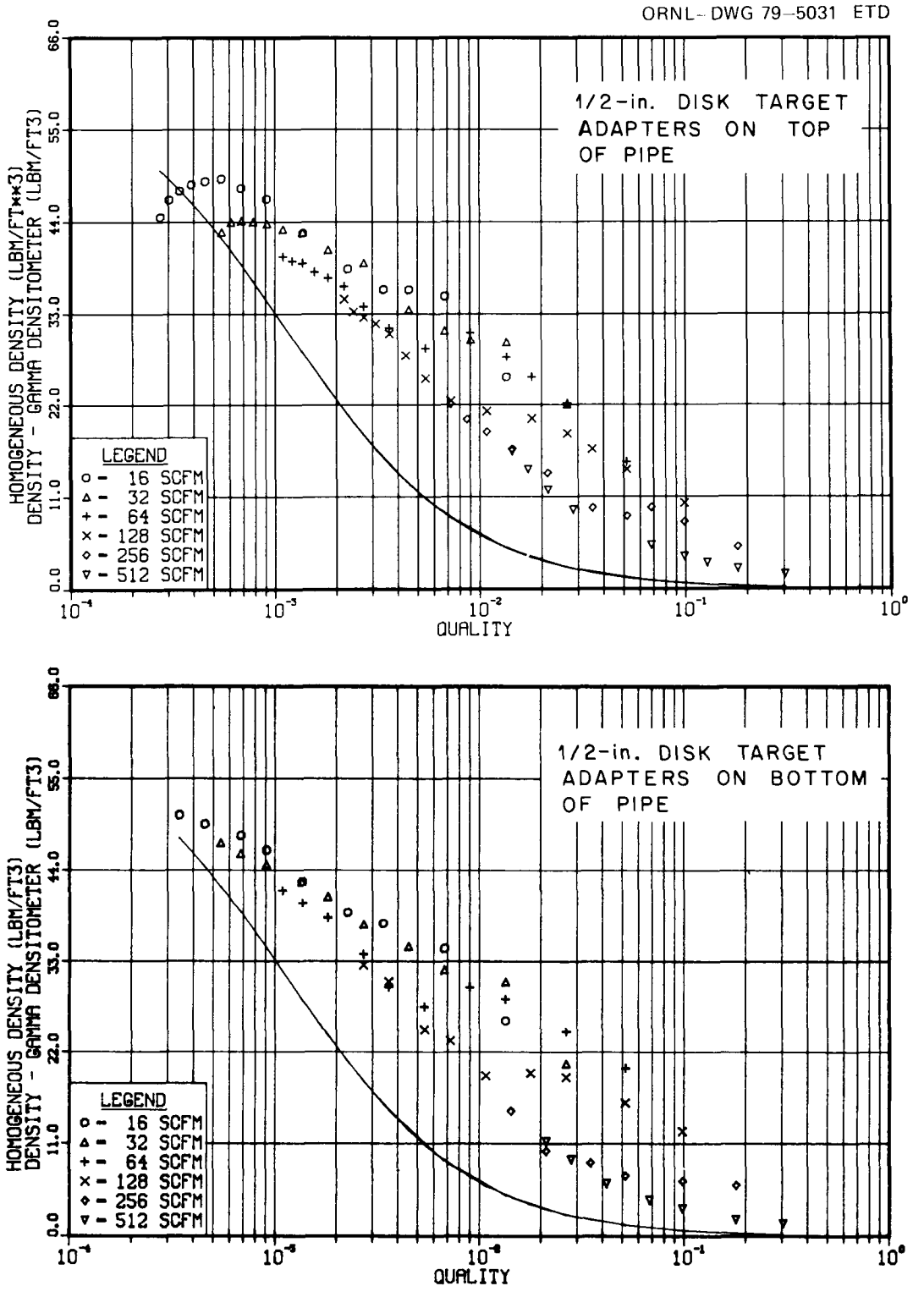

Fig. 4.4. Density drop occurs at low quality when the 1.3-cm (0.5-in.) drag target enters from the top of the test section; density drop does not occur when the 1.3-cm (0.5-in.) target enters from the bottom of the spool piece.

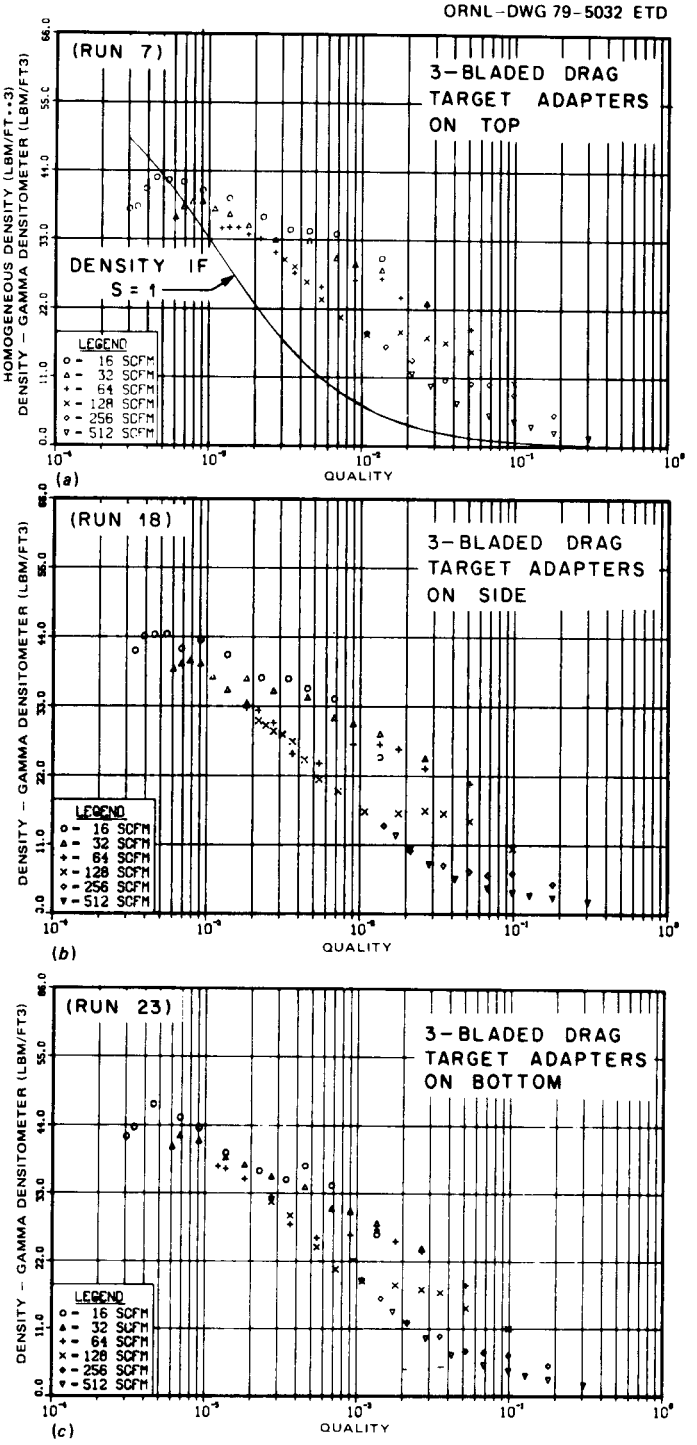

Fig. 4.5. Low-quality density drop is evident with the three-bladed target entering from the top (a) and is still prevalent when the target is entering horizontally (b) and from the bottom (c).

Plots of the turbine meter voltage output (Figs. 4.6 and 4.7) graphically describe the time response of the turbine meter to the passage of a slug. Figure 4.6 also shows that the ORNL electronics for the turbine meter will indicate flow at very low flow rates [velocities <30.5 cm/sec (1.0 fps)].

Calibration of the turbine meter and the two types of electronics has resulted in a conversion equation from voltage output to fluid velocity in feet per second.

$$\text{Vel} = 2.6247 \times \text{Volt} - 0.2181 \ , \tag{4.3}$$

and

$$\text{Vel} = 3.3911 \times \text{Volt} - 0.2181 \ , \tag{4.4}$$

where Eq. (4.4) is for the ORNL electronics package. The improved readings for the turbine meter are not only reflected in tabulated data and velocity plots of the turbine meter, but also in the subsequent calculations for the mass flux in which the turbine meter velocities are used. The mass flux calculation using the equation $G = \overline{\rho V}_t$ is shown in Fig. 4.8. As the flow in the test section decreases and reaches a velocity that the turbine meter electronics cannot interpret, a near-zero or negative value for the velocity is recorded. This erroneous velocity causes the mass flux calculation to be incorrectly near zero or negative. Figure 4.8(a) displays the mass flux calculation using the Flow Technology electronics with the turbine meter, while Fig. 4.8(b) displays the same calculation using the ORNL-developed electronics. The mass flux calculations at higher qualities at 7.55 and 15.1 liters/sec (16 and 32 scfm) noticeably improve the near-zero mass fluxes with the ORNL electronics.

4.2.2 Turbine meter models

The ability of three turbine meter response models to simulate turbine behavior in advanced spool piece I is being studied. The models

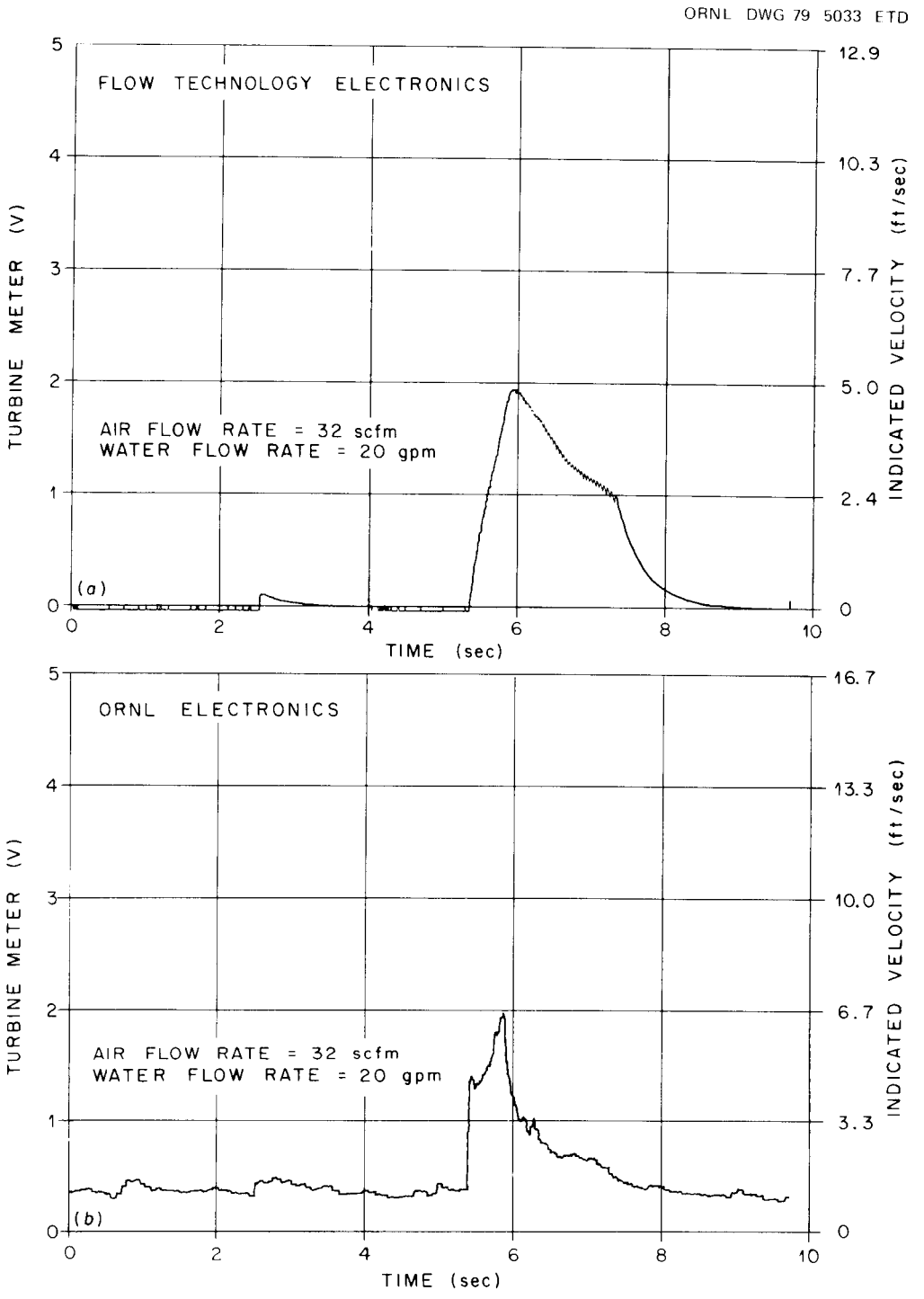

Fig. 4.6. Voltage output of the Flow Technology, Inc., turbine meter electronics (a) and the ORNL-developed electronics (b). Notice the time response of a slow-moving slug at 15.1 liters/sec (32 scfm) and 1.3 liters/sec (20 gpm).

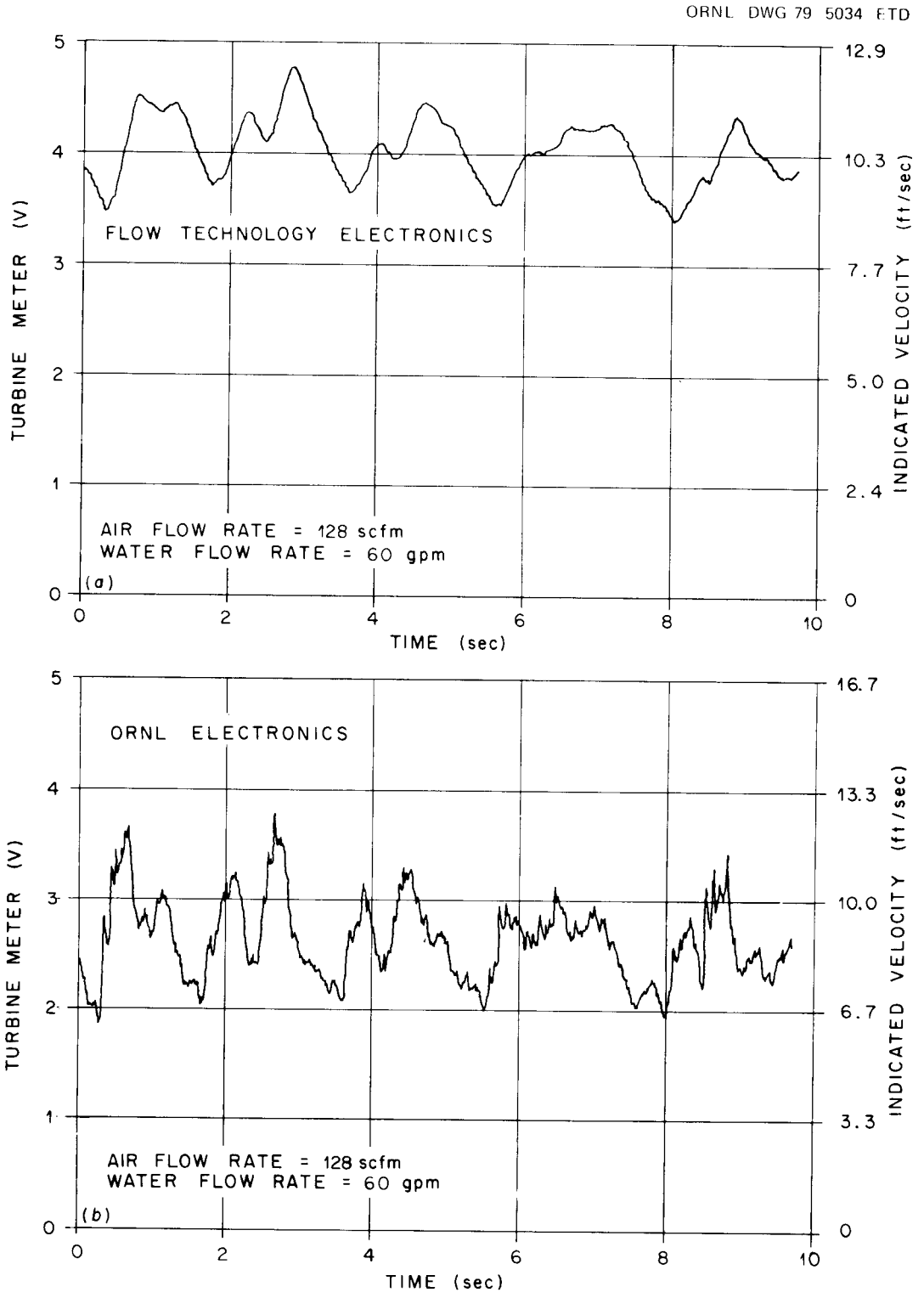

Fig. 4.7. At 3.8 liters/sec (60 gpm) and 60 liters/sec (128 scfm), the time response of the Flow Technology, Inc., electronics (a) is noticeably slower than that of the ORNL turbine electronics (b).

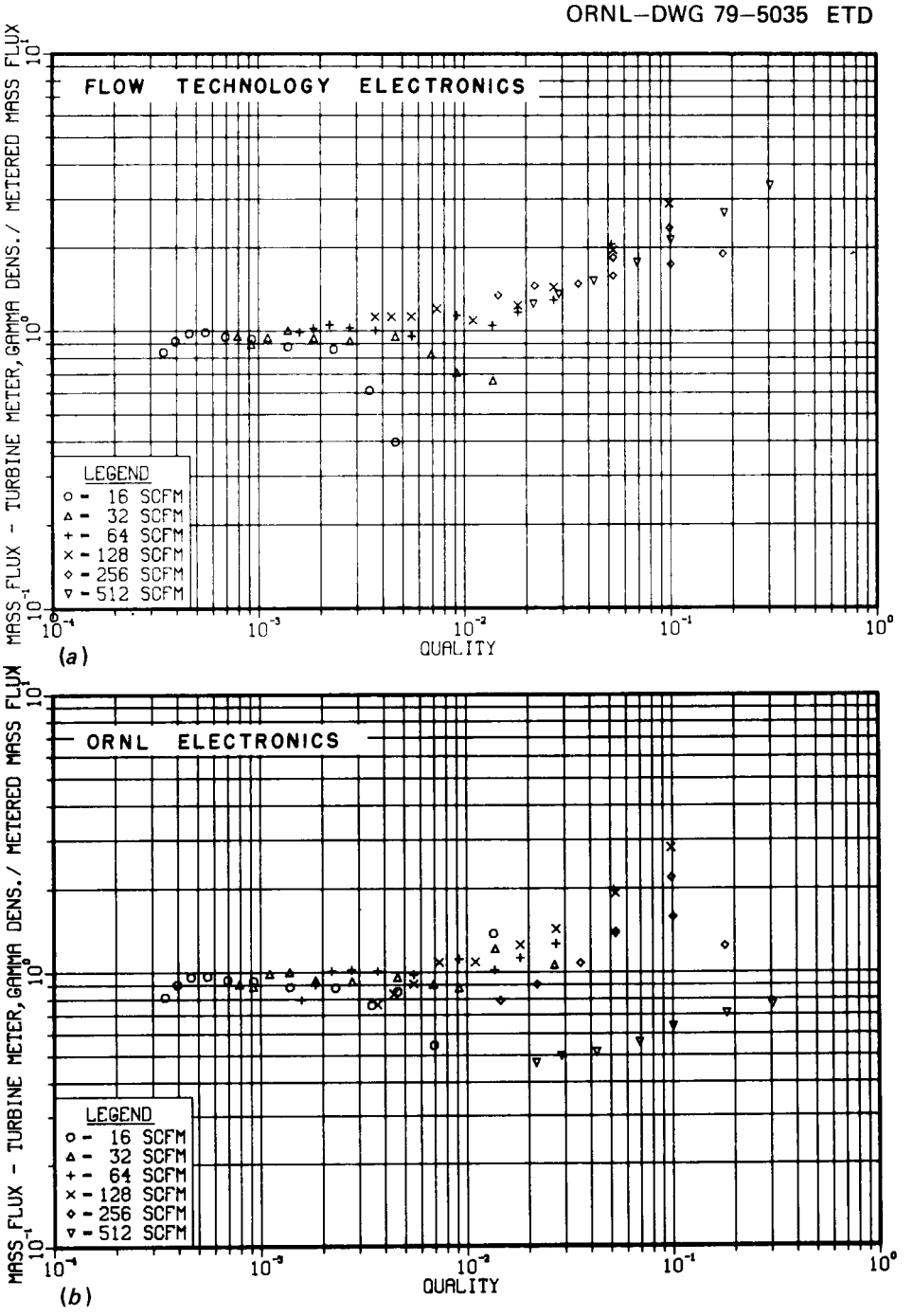

Fig. 4.8. At low air flow rates, the mass flux calculation using the ORNL turbine meter electronics (b) is much improved over the mass flux calculations made using the Flow Technology, Inc. (a) electronics. At 242 liters/sec (512 scfm), the ORNL electronics were overranged.

described by Rouhani,[5] Aya,[6] and the "volumetric"[7] model have been used with data from horizontal two-phase flow experiments in the ORNL air-water loop. The Rouhani and Aya model derivations both assume a twisted turbine blade, which allows the difference between the angular velocity of the turbine blade and the fluid to be uniform on the blade's surface.

Each of the models may be solved for predicted turbine velocity V_t in terms of the densities of the two phases, the mean phase velocities, and the void fraction. For instance, the volumetric model states that

$$V_t = \overline{\alpha V}_g + (1 - \bar{\alpha})\,\bar{V}_f \,, \tag{4.5}$$

where the bars denote an average over a time period and over the pipe cross-sectional area. The Rouhani model assumes a momentum exchange balance on the turbine blades and yields the expression

$$C_f\rho_f(1 - \bar{\alpha})\bar{V}_f(V_t - \bar{V}_f) = C_g\rho_f\overline{\alpha V}_g(\bar{V}_g - V_t) \,, \tag{4.6}$$

where C_f and C_g are drag coefficients for the liquid and vapor phases, respectively, on the turbine blades. Solving for the turbine velocity,

$$V_t = \frac{C_f\rho_f(1 - \bar{\alpha})\bar{V}_f^2 + C_g\rho_g\overline{\alpha V}_g^2}{C_f\rho_f(1 - \bar{\alpha})\bar{V}_f + C_g\rho_g\overline{\alpha V}_g} \,. \tag{4.7}$$

For steady flow and for certain assumptions about "distribution coefficients" and "flow deviation factors," Eqs. (4.6) and (4.7) are in agreement with the Kamath-Lahey turbine model.[8] The Aya model uses a force balance about the turbine blades to obtain

$$C_f\rho_f(1 - \bar{\alpha})(V_f - \bar{V}_f)^2 = C_g\rho_g\bar{\alpha}(\bar{V}_g - V_t)^2 \,. \tag{4.8}$$

Again, this may be solved for the turbine velocity yielding

$$V_t = \frac{-b \pm \sqrt{b^2 - 4ac}}{2a} \,, \tag{4.9}$$

where

$$a = C_g\rho_g\bar{\alpha} - C_f\rho_f(1 - \bar{\alpha}) ,$$

$$b = 2[C_f\rho_f(1 - \bar{\alpha})\bar{V}_f - C_g\rho_g\overline{\alpha V}_g] ,$$

$$c = C_g\alpha\rho g\bar{V}_g^2 - C_f\rho_f(1 - \bar{\alpha})\bar{V}_f^2 .$$

Use of the positive sign in the numerator of Eq. (4.9) gives a solution of Eq. (4.8), but the solution violates the assumption that V_t is greater than $\bar{V}_f$; therefore, the negative sign should be used.

Turbine meter data from run 17 with advanced spool piece I have been compared to the predicted turbine meter readings given by Eqs. (4.5), (4.7), and (4.9). The liquid density used was 1000 kg/m^3 (62.4 lb$_m$/ft^3), and the air density was calculated using

$$\rho_g = 0.071 \frac{P + 14}{14} \text{ lb}_m/\text{ft}^3 , \tag{4.10}$$

where P is the spool piece pressure in psig. The drag coefficients C_f and C_g were assumed constant and equal to unity. The average liquid and vapor velocities were determined from the test data using the void fraction based on the composite density from the densitometer data and the known volumetric inputs of each phase to the loop. The mean velocity of phase i is

$$\bar{V}_i = \frac{Q_i}{A_{tot}\,\bar{\alpha}_i} , \quad \bar{\alpha}_i = \begin{cases} \alpha_g & i = g \\ (1 - \alpha_g) & i = f \end{cases} . \tag{4.11}$$

The spool piece volume fraction $\bar{\alpha}_i$ represents pipe-area averages at the plane of the densitometer and time averages of several thousand readings over 10 or 20 sec. For comparison, time-averaged turbine meter readings were calculated using the ORNL electronics (Sect. 4.2.1) at turbine velocities below 5 m/sec (16 fps) and the Flow Technology electronics at higher velocities. The turbine rotor used did not have twisted blades.

The data shown in Figs. 4.9 through 4.11 are from test 17, which involved horizontal two-phase flow and used a four-bladed drag target, with the drag flowmeter lever arms entering the pipe horizontally. (The effect of the upstream drag target on measured density is described in Sect. 4.1; the effect of the target on turbine meter response in horizontal flow is insignificant.) The flow regimes encountered for these data included stratified, slug, wavy stratified, dispersed, and annular flow (Fig. 2.2).

Mean liquid and vapor velocities calculated using Eq. (4.11) are plotted in Figs. 4.12 and 4.13; the corresponding slip ratio appears in Fig. 4.14.

The results obtained by substituting the mean phase velocities into Eqs. (4.5), (4.7), and (4.9) appear in Figs. 4.9 through 4.11, respectively. In each graph, the abscissa is the mean turbine reading and the ordinate

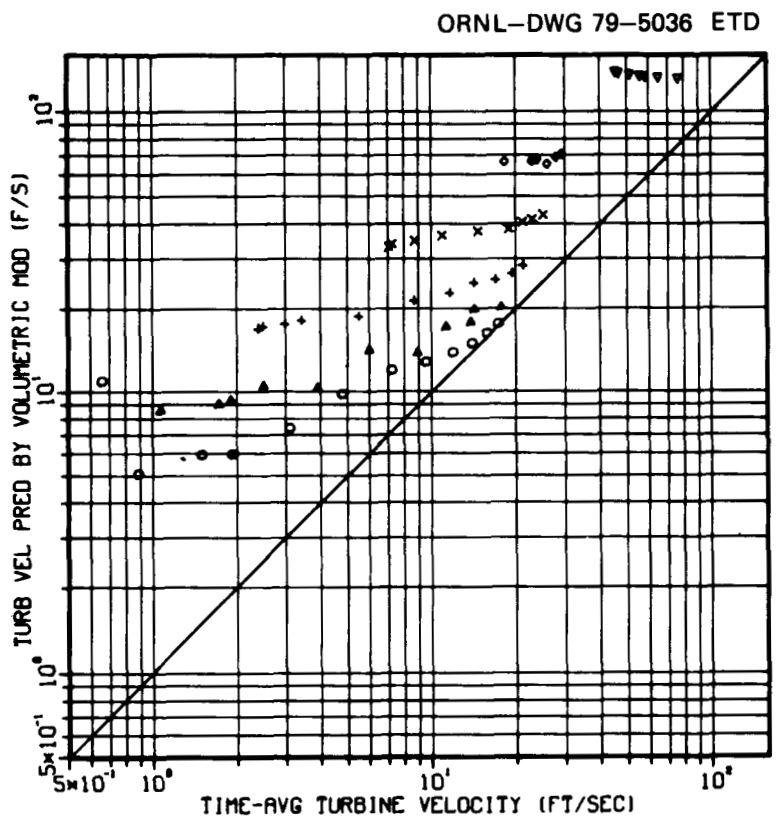

Fig. 4.9. Comparison of turbine velocity predicted by volumetric model to mean turbine velocity, run 17.

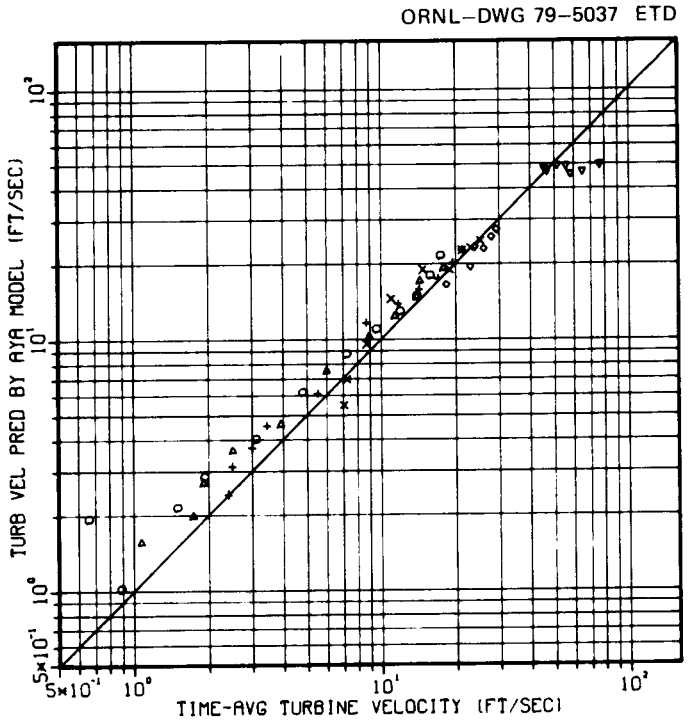

Fig. 4.10. Comparison of turbine velocity predicted by Aya model to mean turbine velocity, run 17.

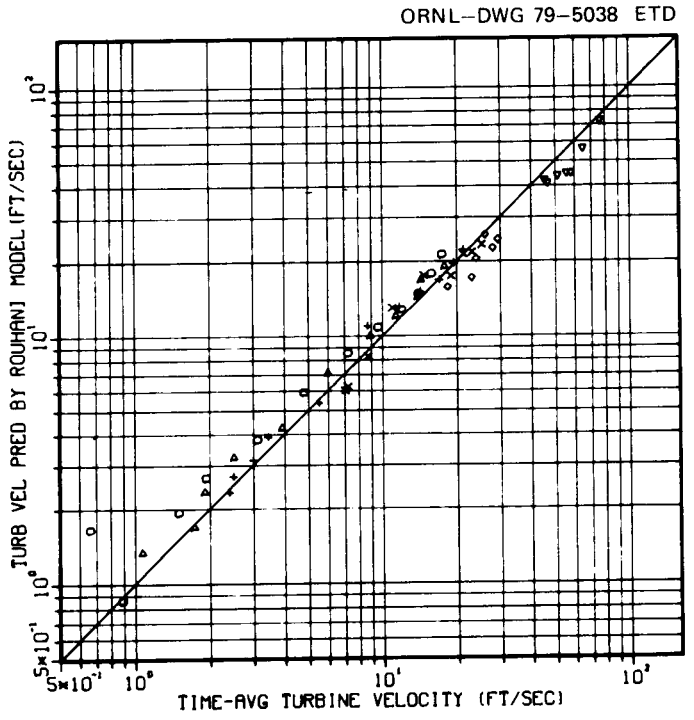

Fig. 4.11. Comparison of turbine velocity predicted by Rouhani model to mean turbine velocity, run 17.

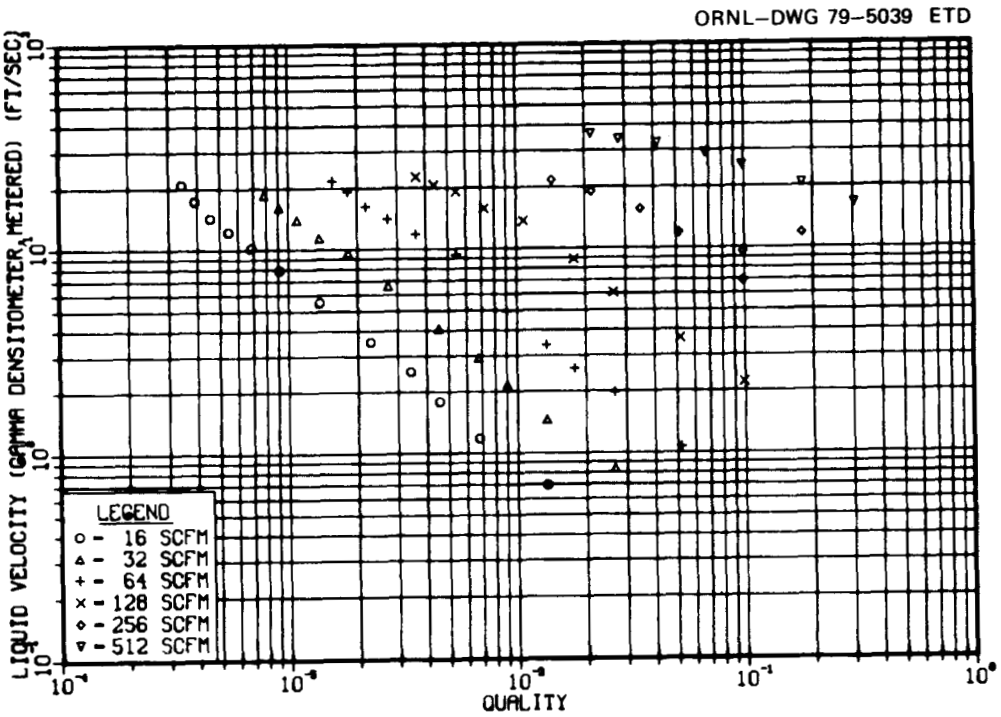

Fig. 4.12. Mean liquid velocity V_f, run 17, plotted vs quality.

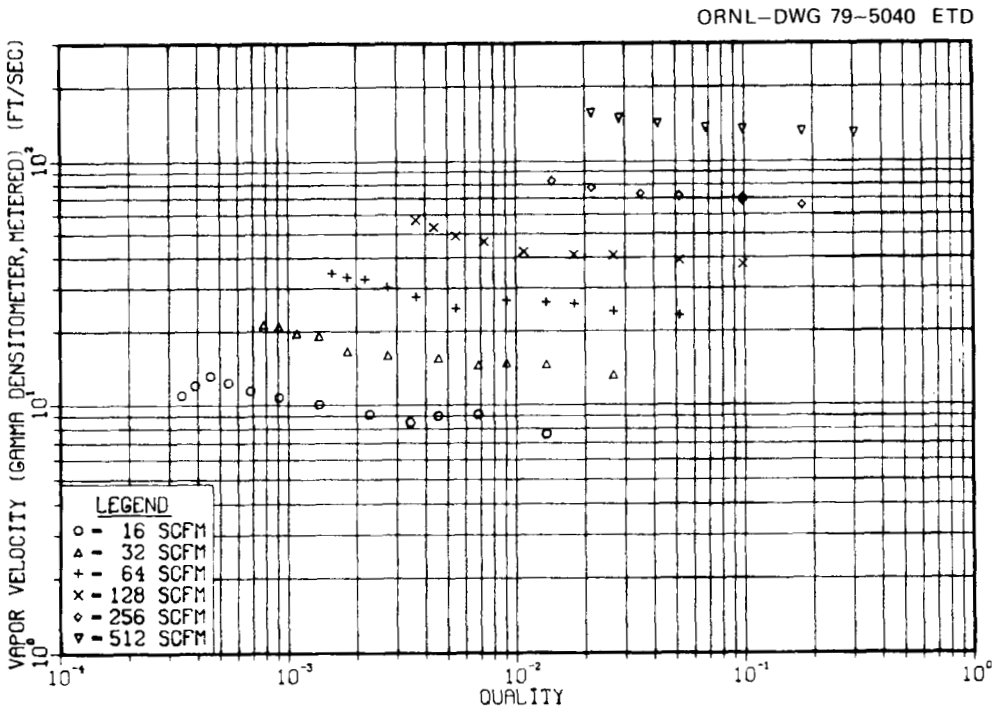

Fig. 4.13. Mean vapor velocity V_g, run 17, plotted vs quality.

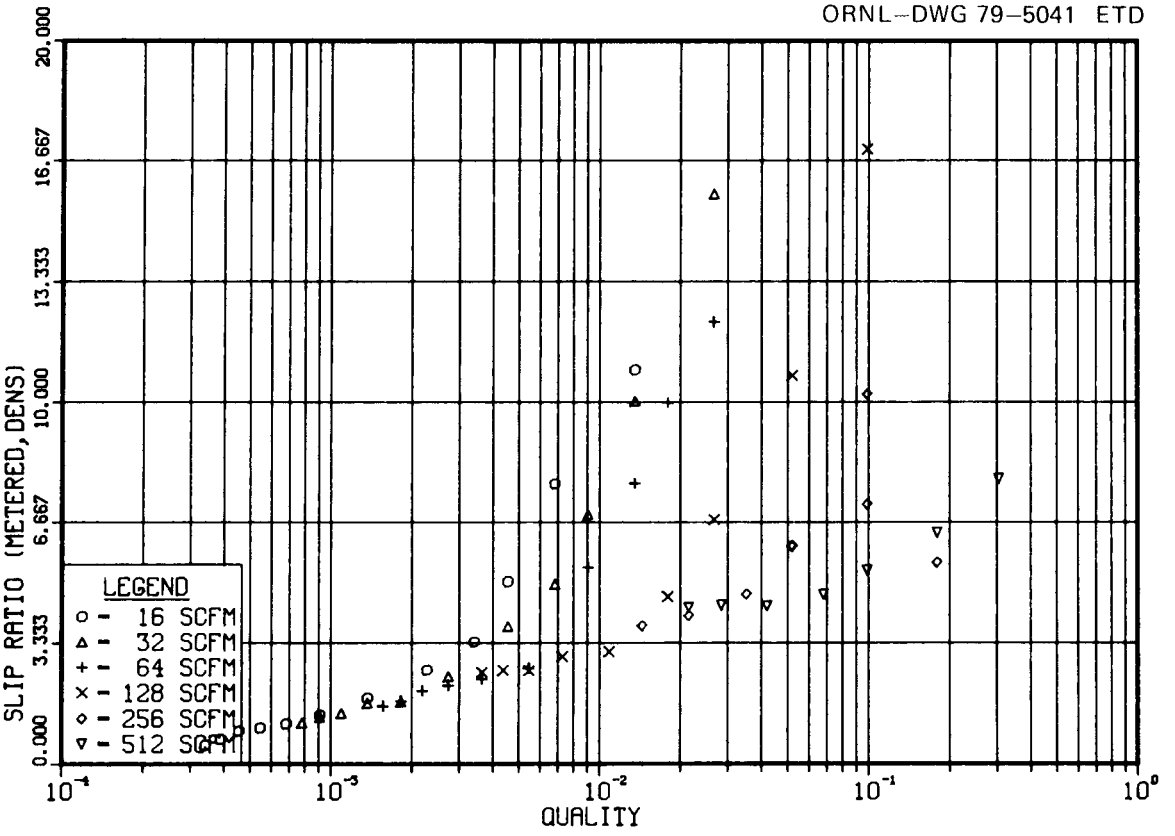

Fig. 4.14. Slip ratio (V_g/V_f), run 17, plotted vs quality.

is the turbine reading predicted by one of the three models. The volumetric model (Fig. 4.9) badly overestimates the turbine velocity for the horizontal flow data, often predicting velocities two or three times the measured values. In contrast, both the Aya (Fig. 4.10) and the Rouhani (Fig. 4.11) models estimate the observed turbine velocities well. In general, they slightly overpredict the observed turbine velocities at the lower air flow rates (stratified and slow slugging flow regimes) and slightly underpredict the observed values at the higher air flow rates (annular and fast slugging flow regimes). As an estimator of the goodness-of-fit of the models to the data, the quantity

$$\sigma \equiv \left[\frac{1}{N-1} \sum_{i=1}^{N} \left(\frac{V_{tmod}}{V_{tact}} - 1 \right)^2 \right]^{1/2} \qquad (4.12)$$

was calculated. The results were σ = 251% for the volumetric model; σ = 21.8% for the Aya model; and σ = 15.9% for the Rouhani model.

In applying these results to other two-phase systems, remember that there is a very large difference between the phase densities in the air-water loop. In this study, the terms in Eqs. (1), (2), and (5), which are multiplied by ρ_g, only become significant at high gas velocities. In a two-phase system at high pressure, the density ratio ρ_g/ρ_f may be much larger, and the effects of the gas velocity on the turbine may be important over a much wider range of flow rates.

4.3 Drag Flowmeter

4.3.1 Background

A goal of the current testing is the evaluation of various drag body designs in terms of their suitability for two-phase momentum flux measurements. The drag target designs being tested with the Ramapo Mark V drag flowmeter transducer are shown in Fig. 4.15; pertinent information about them is given in Table 4.1. The targets tested were intended to represent typical designs in use or proposed for two-phase momentum flux measurements in reactor safety studies. [Results from vertical downflow air-water studies with target numbers 7, 8, and 9 have been reported by Sheppard.[9] A "Maltese cross" or blade-type target has been tested in single-phase water and steam-water (steady state) by Columbia University and Combustion Engineering.[10] A full-flow target (one which samples essentially the entire pipe cross section) of perforated plate design has been used by Fincke in two-phase air-water[11] and in a blowdown facility.[12]]

A number of approaches may be taken to evaluate the "true" momentum flux in a two-phase system. Andeen and Griffith[13] have used the deflection of a tee to measure momentum flux in a steam-water system; they did not use a drag flowmeter for comparison, however. A Pitot tube rake was used by Fincke[11] to calculate momentum flux profiles in horizontal air-water flow for comparison with the cross-sectional average momentum flux

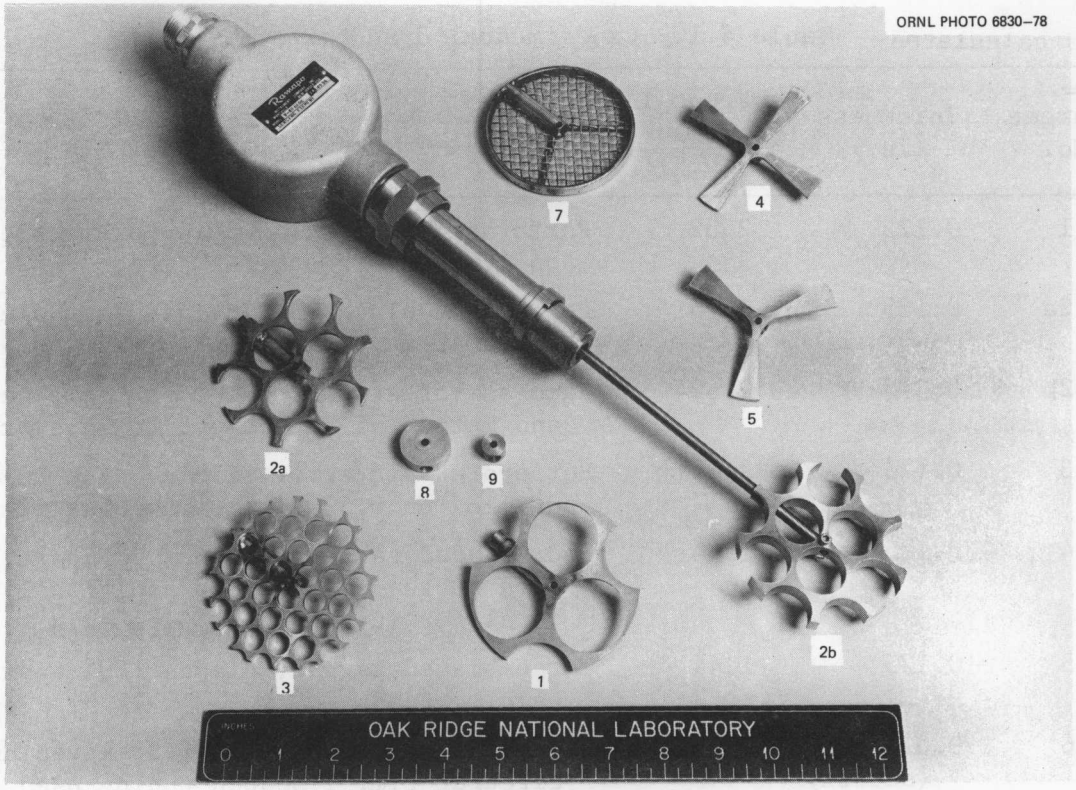

Fig. 4.15. Ramapo Mark V drag flowmeter and experimental drag targets (Table 4.1).

determined by a drag screen. Sheppard et al.[9] compared their drag flowmeter readings to momentum fluxes determined from a turbine meter using the Rouhani[5] and Aya[6] models. In addition, the reduced drag flowmeter reading I_D has been combined with either a measured density or a measured velocity to yield a mass flux.[14] When the actual mass flux is known and the density and velocity measurements are interpreted correctly, an evaluation of the drag target performance may be made.

4.3.2 Momentum flux calculation methods

In the current study, all the targets in Fig. 4.15 were tested in horizontal two-phase air-water flow; besides the drag flowmeter output, turbine meter, three-beam densitometer, and pressure-drop data were recorded. The instrument electronics, data acquisition system, and some data reduction techniques used have been described previously.[3]

Table 4.1. Experimental drag targets[a]

Target No.	Thickness (in.)	Frontal area[b] (in.^{2})	Description
1	0.125	2.32	Perforated plate, 1.375-in.-diam holes on 1.56-in. triangular pitch
2a	0.125	2.75	Perforated plate, 0.938-in.-diam holes on 1.040-in. triangular pitch
2b	0.375	2.624	Same as target 2a, except for thickness and method of attachment to lever rod
3	0.125	2.851	Perforated plate, 0.4375-in.-diam holes drilled on 0.500-in. triangular pitch
4	0.125	1.44	Four-bladed target, blades 90° apart, each subtends 15°; some additional metal for support near pipe axis
5	0.125	1.44	Three-bladed target, blades 120° apart; each subtends 20°
6	0.025 (screen) 0.125 (rim)	2.099	Five-mesh screen held in 2.25-in.-diam circular rim; Y-shaped tubing used for support
7	0.025 (screen) 0.125 (rim)	3.642	Five-mesh screen held in 3.28-in.-diam circular rim; Y-shaped tubing used for support
8	0.375	1.067	1-in.-diam disk
9	0.375	0.5339	0.50-in.diam disk

[a] 1 in. = 2.54 cm; 1 in.^{2} = 6.45 cm^2.

[b] Includes frontal area of mounting tubes or support rod directly exposed to flow.

During the current studies, no direct momentum flux measurements were made, except those from the drag flowmeter. Two methods involving the turbine meter, gamma densitometer, and the metered single-phase volumetric input rates to the loop were used to estimate the two-phase momentum flux in the test section. Both methods include the assumption that the momentum flux may be calculated from

$$M = (1 - \alpha)\, \rho_f V_f^2 + \alpha \rho_g V_g^2 \,, \tag{4.13}$$

where the phase velocities V_f and V_g are mean values over the pipe cross section and over the scan time. The first technique uses the void fraction α calculated from the densitometer[3] to obtain

$$M_1 = 1/A^2 \left(\frac{\rho_f Q_f^2}{1 - \alpha} + \frac{\rho_g Q_g^2}{\alpha} \right) , \tag{4.14}$$

where Q_f and Q_g are the volumetric input rates of liquid and vapor to the loop, respectively. The second method uses the Aya model turbine meter equation,[6]

$$\alpha\rho_g (V_{g_{Aya}} - V_t)^2 = \rho_f (1 - \alpha)(V_t - V_{f_{Aya}})^2 \tag{4.15}$$

and the equations of continuity for each phase to calculate $V_{f_{Aya}}$ in terms of the mean turbine reading V_t and the input mass flow rates to the loop. The vapor velocity $V_{g_{Aya}}$ is then calculated using

$$V_{g_{Aya}} = \frac{G_g \rho_f V_{f_{Aya}}}{\rho_g \rho_f V_{f_{Aya}} - \rho_g G_f} , \tag{4.16}$$

where G_g and G_f are the mass fluxes of vapor and liquid, respectively. The void fraction is

$$\alpha_{Aya} = \frac{\dot{m}_g}{\rho_g V_g} . \tag{4.17}$$

Finally V_f, V_g, and α are substituted into Eq. (4.13) to give

$$M_2 = (1 - \alpha_{Aya}) \rho_f V_{f_{Aya}}^2 + \alpha\rho_g V_{g_{Aya}}^2 . \tag{4.18}$$

The previous quarterly report[3] shows that the two-phase mass flux calculated as $G_3 = I_d/V_T$ conforms to the assumption implied by Eq. (4.13) for drag flowmeter behavior and to the assumption of Rouhani and Estrada[15] for turbine meter behavior. We have also found (Sect. 4.2.2) that the Rouhani turbine model performs well in the horizontal two-phase studies. Comparisons of G_3 to the actual mass flux may then be used to evaluate drag target behavior in the air-water system. Conversely, the calculation of mass flux using the equation $G = (\rho_a I_d)^{1/2}$ does not agree with the two-velocity mass flux calculation

$$G = \alpha\rho_g V_g + (1 - \alpha)\rho_f V_f \tag{4.19}$$

and thus is not useful for evaluation of drag target behavior (Sect. 5.1).

4.3.3 Target design experiments

In horizontal two-phase flow, the shape of the drag target may be important because of asymmetry of void fraction, velocity, etc., with respect to the pipe axis. When the drag flowmeter lever arm is mounted vertically, this asymmetry influences the effective length of the lever arm and, thus, the measured force. When the lever arm enters the pipe horizontally, these errors are minimized. (Fincke[11] has shown that, with horizontal lever arm orientation, errors caused by proximity of upstream bends may be neglected for full-flow targets.)

As part of the current studies, the spool piece has been rotated about its axis, and data have been taken with the drag flowmeter adapters on top, on the side, and on bottom of the pipe. Because of the design of advanced spool piece I, with pressure taps on the side of the spool piece opposite the drag adapters, most runs comparing the various targets and the effects of flow-dispersing screens have been made with the drag adapters on top of the pipe.

In Fig. 4.16, M_1, the two-velocity momentum flux based on the measured void fraction, is graphed vs M_2, the two-velocity momentum flux calculated from turbine meter data using Aya's turbine model. The agreement for run 7 is quite good, as it was for all the tests run. The

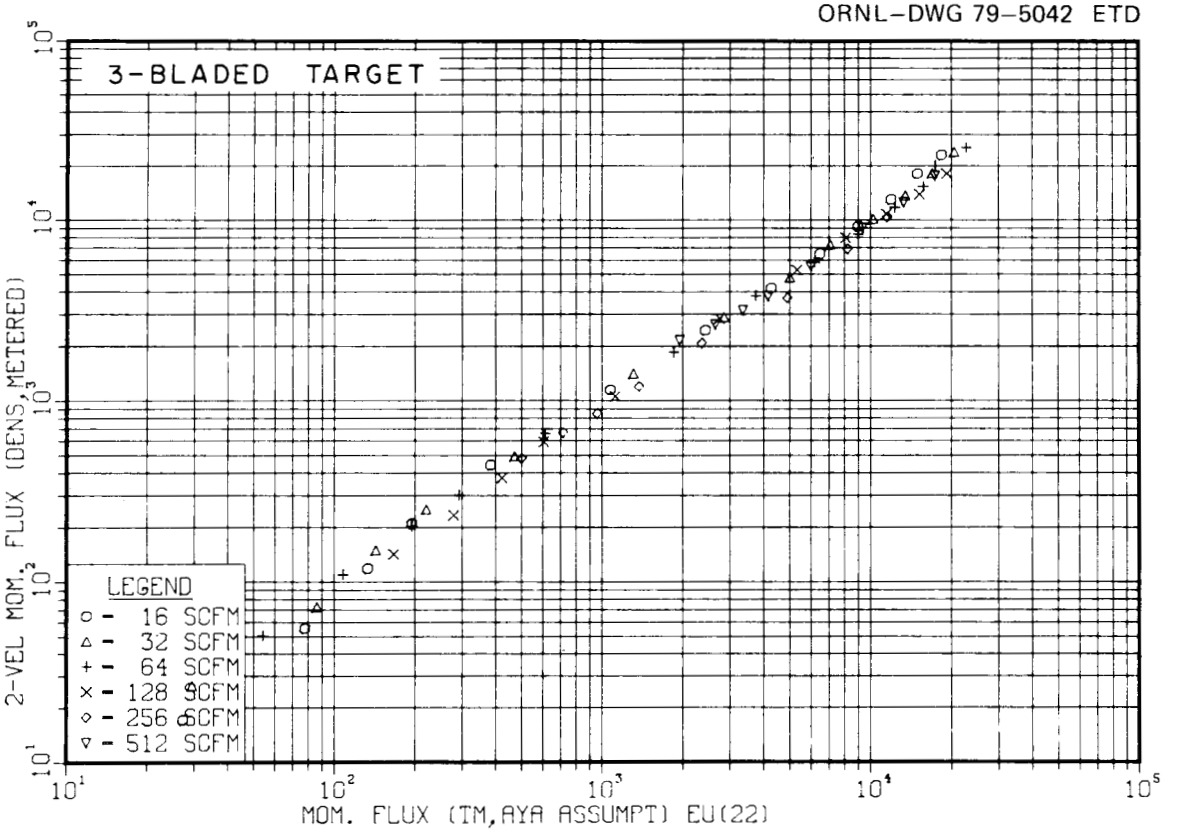

Fig. 4.16. M_1 [Eq. (4.14)] vs M_2 [Eq. (4.18)], run 7.

momentum flux calculated using the measured void fraction M_1 was also compared to the mean pressure drop across a 4-20 screen (four stacked layers of 20-mesh per inch screen) (Sect. 4.4). Except at very low pressure drops, the two sets of data have a linear relationship, suggesting that M_1 is directly proportional to the actual momentum flux.

In the following discussion, the definitions

$$R_1 \equiv I_d/M_1 \ ,$$

$$R_2 \equiv I_d/M_2 \ , \qquad (4.20)$$

$$R_3 \equiv G_3/G_{actual}$$

will be used.

To illustrate the results obtained from the full-flow drag targets tested, plots of the ratios R_1, R_2, and R_3 will be shown for one of the better targets, the three-bladed one, and one of the worst targets, the large-holed perforated plate.

Figure 4.17 shows R_1 vs quality from run 7. The predominance of data is between 0.75 and 1.2, but several points are higher, between 1.2 and 3.5. R_2 (Fig. 4.18) behaves similarly for the three-bladed target, with fewer points lying greater than 1.2. Overestimation of the two-velocity momentum flux at low air flow rates with low water flow rates occurred consistently for all targets tested; that is, R_1 and R_2 were significantly greater than unity for all targets at those flow rates. This behavior is probably not caused by inconsistent drag target or transducer performance, but rather is caused by the occurrence of slug flow with low slug frequency. As was shown in the previous quarterly

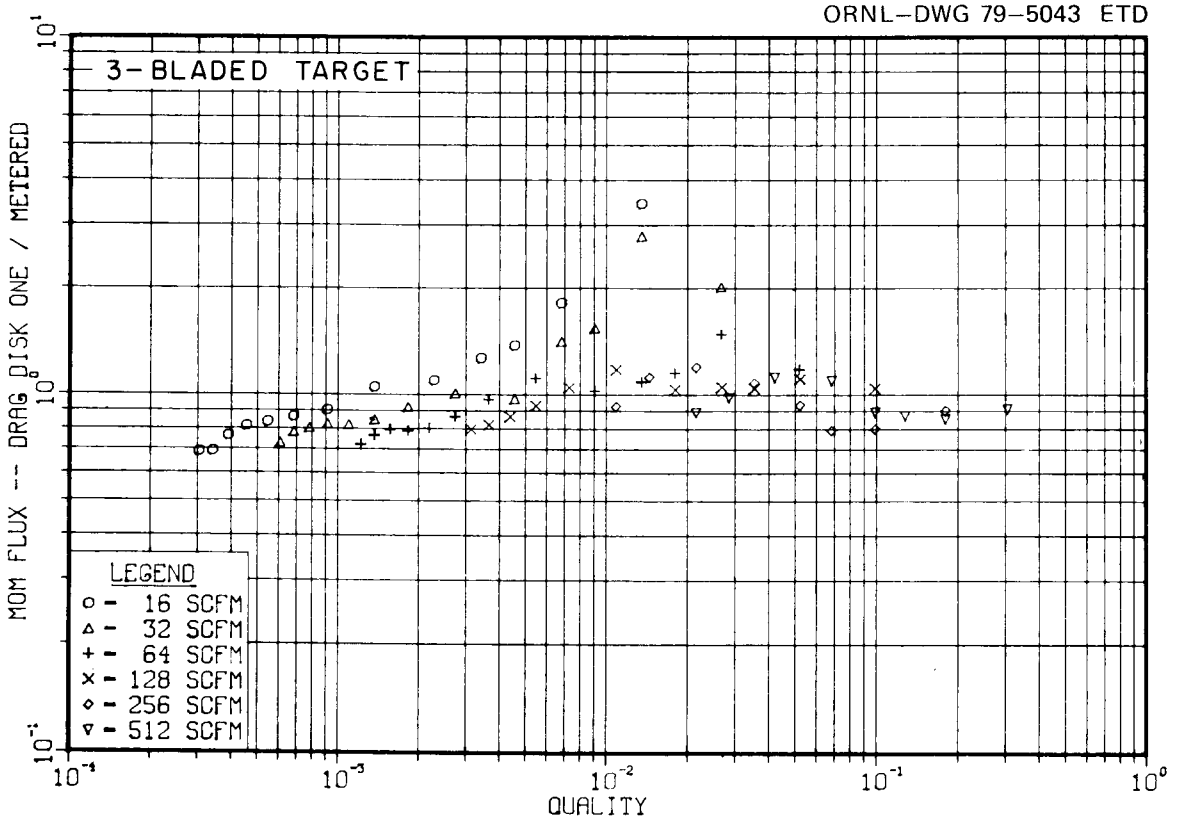

Fig. 4.17. R_1 vs quality, run 7, three-bladed target.

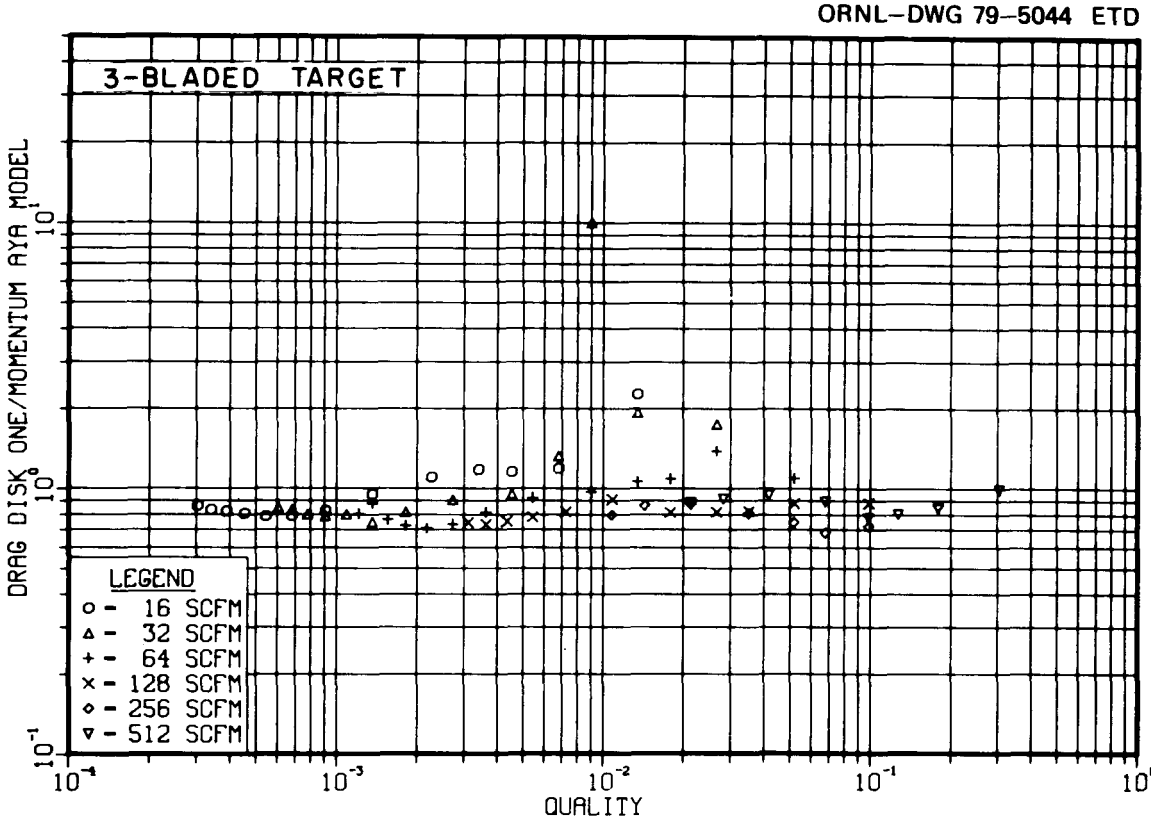

Fig. 4.18. R_2 vs quality, run 7, three-bladed target.

report,[3] the majority of momentum flux detected during a scan at low flow rates comes from the passage of a few rapidly moving slugs of water. The two-velocity assumption of uniform volumetric air and water flow rates with time throughout the system is violated when a slug of water fills the pipe and is accelerated by air trapped behind it. In the calculation of M_1, the reduced (or zero) void fraction detected upon passage of a slug is interpreted as a drop in liquid velocity from that occurring during quiescent stratified flow between slugs. On the other hand, the turbine meter velocity increases upon passage of a slug, but the Aya turbine assumption may be poor during that period, again causing an underestimate of the slug momentum in the calculation of M_2. The underestimate is less serious for M_2 (Fig. 4.18) than for M_1 (Fig. 4.17). The mass flux ratio R_3 based on the drag flowmeter and turbine meter readings (Fig. 4.19) generally lies between 0.7 and 0.9 for the three-

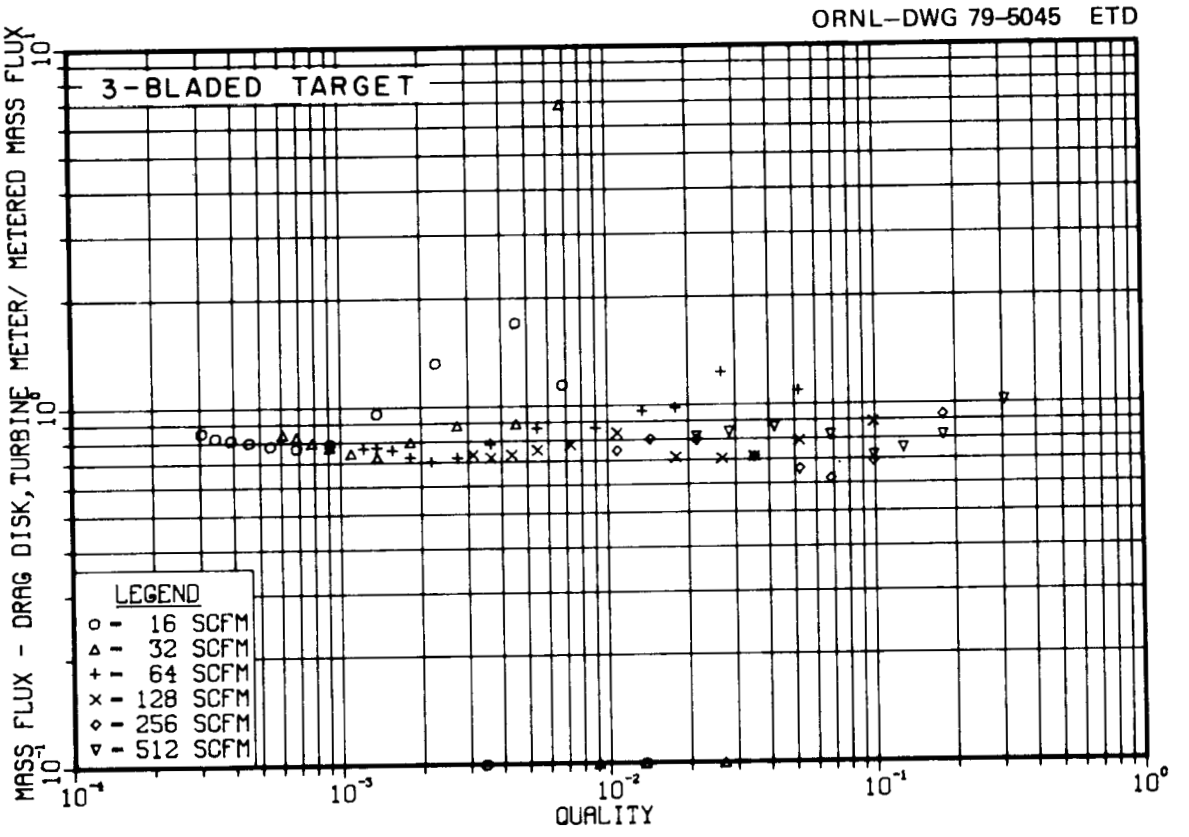

Fig. 4.19. R_3 vs quality, run 7, three-bladed target.

bladed target. Larger ratios occurred when the turbine meter signal was intermittent.

Probably the worst performance of the full-flow targets tested was that of the perforated plate target with large holes. The ratios R_1, R_2, and R_3 for run 13 with the large-holed target are shown vs quality in Figs. 4.20 through 4.22. As can be seen, there is much more scatter in the data for R_1 (Fig. 4.20) for this target than for the three-bladed target (Fig. 4.17), especially at low qualities. Most of the data for R_2 (Fig. 4.21) lie between 0.6 and 1.0, only slightly worse than R_2 for the three-bladed target (Fig. 4.18). However, R_3 (Fig. 4.22) is clearly worse with the perforated plate, ranging from ∿0.55 to over 1.0.

Preliminary analysis indicates that several of the targets tested behave similarly. In fact, data for the three-bladed and four-bladed targets, the small-rimmed screen, and the perforated plate targets with intermediate-sized holes are very difficult to distinguish without more

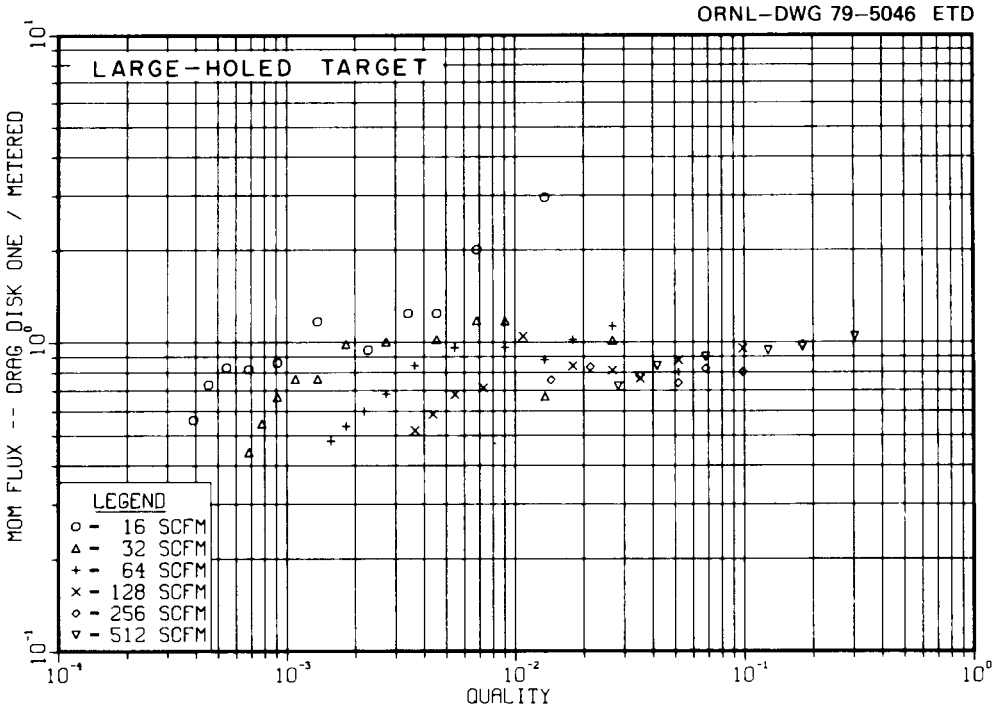

Fig. 4.20. R_1 vs quality, run 13, large-holed target.

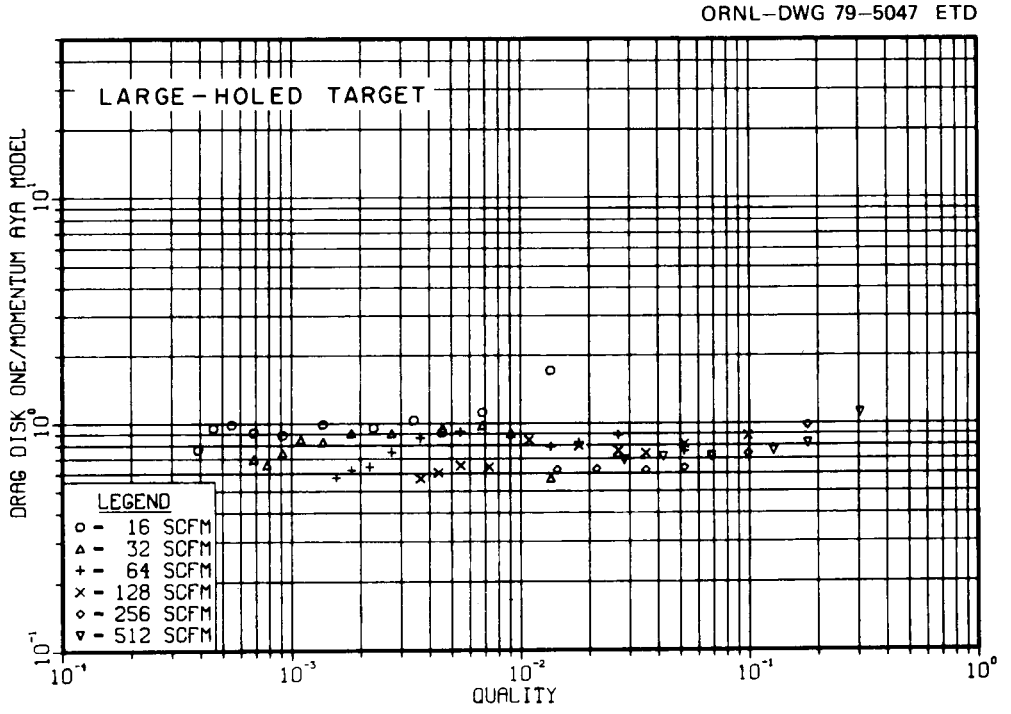

Fig. 4.21. R_2 vs quality, run 13, large-holed target.

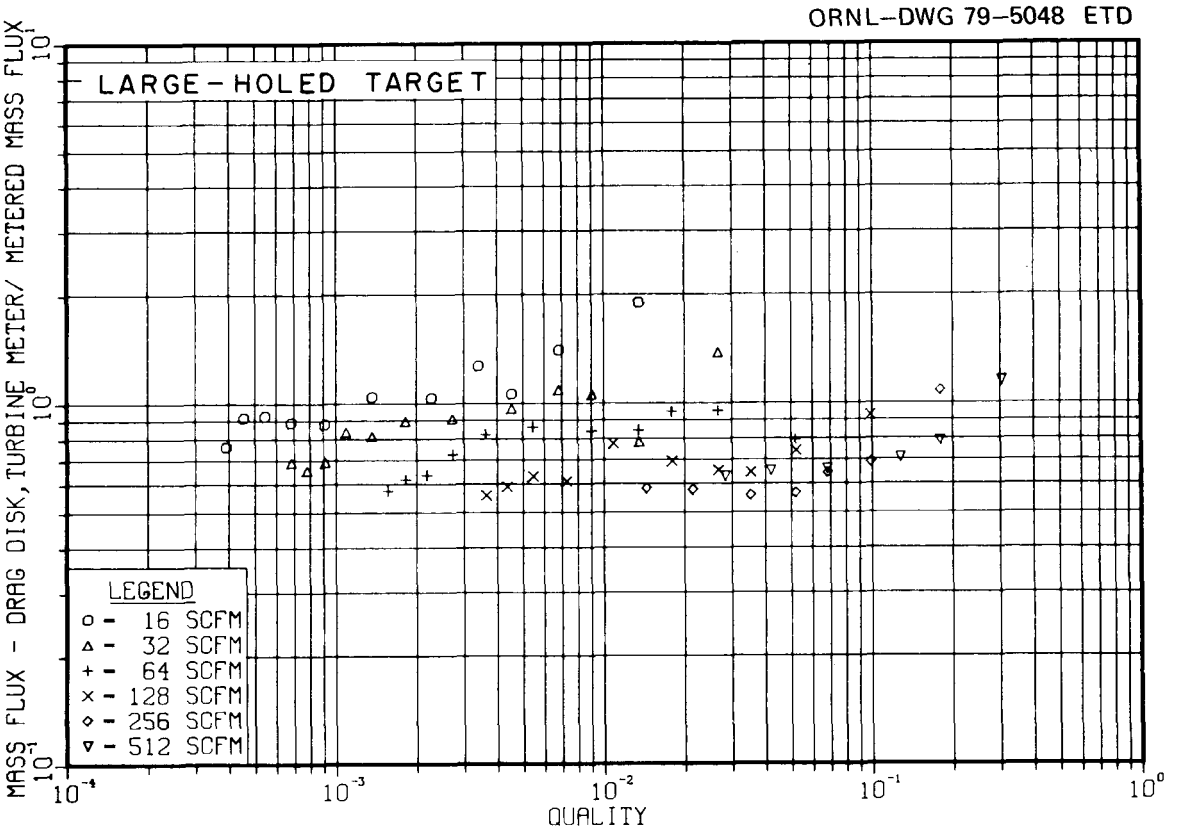

Fig. 4.22. R_3 vs quality, run 13, large-holed target.

detailed statistical analysis. There was essentially no difference in two-phase flow performance between the thick and the thin perforated plate targets with intermediate-sized holes. (Both targets had the same hole pattern.) The 2.54-cm (1-in.) disk and the perforated plate-type targets with large holes and with small holes do noticeably poorer in terms of nearness of R_1, R_2, and R_3 to unity over the range of flows tested.

Another common characteristic of all the targets has been the consistent grouping of the mean of R_1, R_2, or R_3 at values below 1.0. For the three-bladed target (Figs. 4.17 through 4.19) the means of R_1, R_2, and R_3 are 0.94, 0.86, and 0.82, respectively. [Data at water flow rates below 3.8 liters/sec (60 gpm) at air flow rates of 7.55 and 15.1 liters/sec (16 and 32 scfm) were omitted.] This suggests that the drag coefficients of all the targets may be considerably less for two-phase flow than for single-phase flow. Similar results have been obtained

for one-component systems at near saturated conditions. For example, in fully cavitating three-dimensional flow, the drag coefficient of a thin disk has been found to be ∿0.80, while, in single-phase flow, the same disk has a drag coefficient of ∿1.17.[16]

4.3.4 Low air-flow experiment

For the purpose of calculating a momentum flux from the voltage output of the drag flowmeters, the drag coefficient in two-phase flow has been assumed to be constant and equal to that in the single-phase flow. Discussions in a previous section indicate that the assumption of the two-phase drag coefficient being constant and equal to the single-phase C_D is not correct. One experiment to test the constant C_D assumption was a low air-flow performance test of a four-blade drag flowmeter target in vertical downflow. At a steady liquid flow of 25.2 liters/sec (400 gpm), the drag flowmeter, densitometer, and turbine meter readings were recorded at air flow rates varying from 0 to 7.55 liters/sec (0 to 16 scfm).

Table 4.2 shows the two-velocity momentum flux M_1 calculated by using Eq. (4.14) and the voltage output signal (proportional to the drag force) of the drag flowmeter. Because the drag coefficient[17] is defined by

Table 4.2. Analysis of low air flow data at 25.2 liters/sec (400 gpm)[a]

Air flow rate [liters/sec (scfm)]	Void fraction (α)	Momentum flux ($lb_m/ft\text{-}sec^2$)	Drag flowmeter output (V)	Density (lb_m/ft^3)
0 (0)	0.0	11,105	5.96	62.3
0.944 (2)	0.02	11,349	6.09	60.73
1.888 (4)	0.05	11,691	6.15	58.95
3.776 (8)	0.15	13,114	6.32	52.50
7.552 (16)	0.44	20,050	6.73	34.36

[a] 1 $lb_m/ft\text{-}sec^2$ = 1.49 kg/m^2; 1 lb_m/ft^3 = 16 kg/m^2.

$C_D = (F/A_t)/\dot{M}$, one can observe that as the void fraction increases, the drag coefficient decreases. This decrease is more noticeable at 3.78 and 7.55 liters/sec (8 and 16 scfm), suggesting that the drag coefficient is not a constant value in two-phase flow. Air is possibly being trapped behind the drag target, producing an aerodynamic shape (which causes a streamlined action of the flow across the drag target) and reducing the amount of drag on the body.

Further studies of the drag coefficient of the drag targets in two-phase flow are being conducted.

4.3.5 Effects of flow-dispersing screens

Several air-water experiments have been run with flow-dispersing screens at the upstream flange of the spool piece (Fig. 1.1). Again, flow was horizontal, and the drag flowmeter adapters were on top of the pipe. Previous work has indicated that screens have a beneficial effect on drag flowmeter performance in vertical downflow[18] but cause little improvement in performance in horizontal flow.[19] The earlier studies involved use of a 1.3-cm (0.5-in.) drag target; the effects of screens on the larger targets are now being studied.

Runs with a 4-20 flow-dispersing screen upstream of the drag flowmeters were made using the 1.3-cm (0.5-in.) disk, 2.54-cm (1-in.) disk, and three-bladed target. A 2-20 screen was also tried with the three-bladed targets, and one run was made with a 4-20 screen at the upstream flange and the central screen location, between the densitometer plane and the turbine meter (Fig. 1.1). In all cases, no significant improvement in drag flowmeter performance occurred when the screens were used, based on plots of R_1, R_2, and R_3.

A discussion of the effects of flow-dispersing screens on pressure drop measurements is found in Sect. 4.4.

4.3.6 Comparison of two drag flowmeters

The location of a second drag flowmeter in advanced spool piece I was intended primarily to ensure that, during periods of reverse flow,

one drag meter would be upstream of the turbine meter. In vertical downflow, it has been shown[18] that location of the drag flowmeters [with a 1.3-cm (0.5-in.) target] downstream of a turbine can result in very poor momentum flux measurements.

Single-phase data recorded from the downstream drag flowmeter (hereafter referred to as DF2) were used to reduce two-phase flow data from that meter. In general, the calibration coefficients used were somewhat different from those used for DF1, when the same target type was used for both meters. Using an equation of the form $I_d = aV^b$ for the momentum flux in terms of voltage output, the factor a was typically lower for DF2 than for DF1 by ∿10%. The value of b for DF1 was always ∿1.00, but b for DF2 was usually much greater.

A plot of R vs quality for DF2 from run 7, which used three-bladed targets, appears in Fig. 4.23. Compared with R_1 from DF1 in run 7

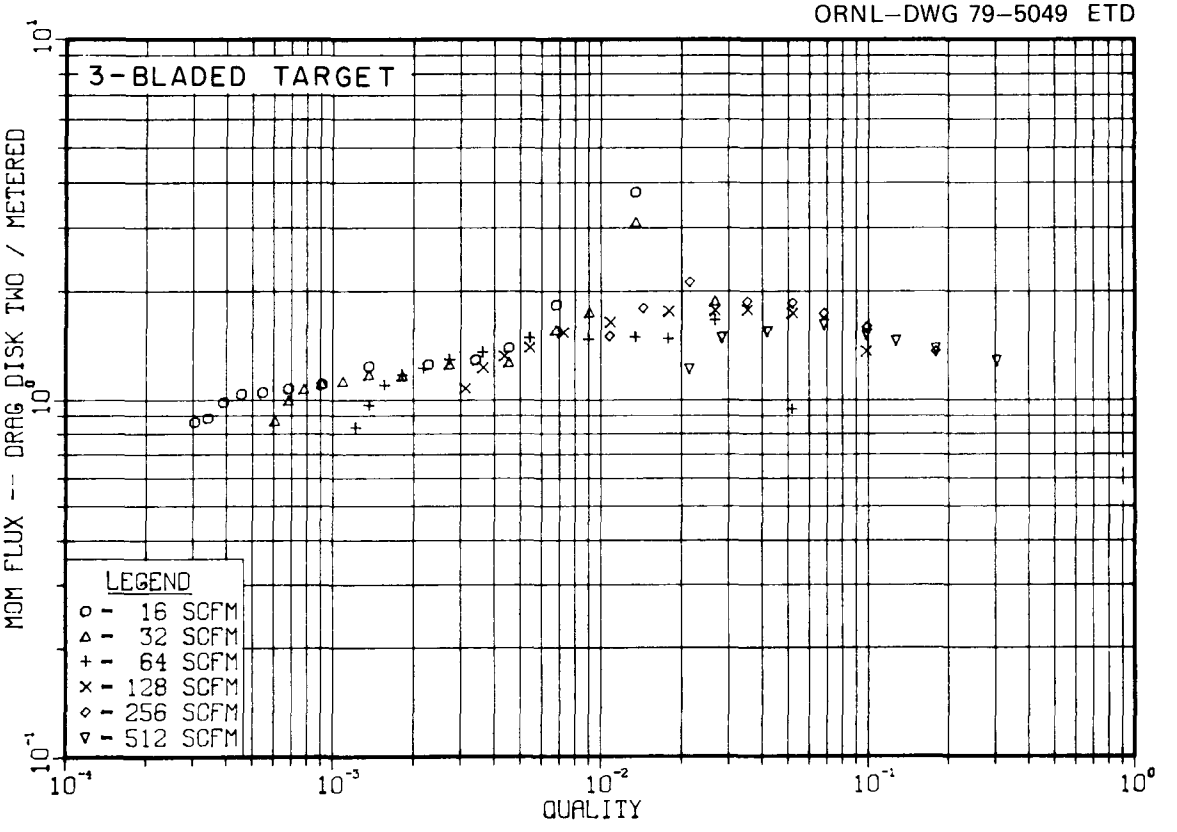

Fig. 4.23. R_1 vs quality, run 7, data from downstream drag flowmeter (DF2), with three-bladed target.

(Fig. 4.17), one sees that the behavior is similar, although DF2 tends to overpredict the two-velocity momentum flux more severely in the quality range above 1%. This behavior occurred consistently for all runs with all target types tested. It was not affected significantly by the presence of a flow-dispersing screen either at the upstream flange or in the center of the spool piece. However, the full-flow targets clearly perform significantly better than the 1.3-cm (0.5-in.) disk, when located downstream of a turbine. A drag flowmeter located downstream of a turbine could be used to complement data from one upstream of a turbine, at least in horizontal flow. Use of a design such as that of advanced spool piece I, with a drag flowmeter on each end, is recommended in locations where flow reversals are likely to occur.

4.3.7 Effects of drag adapter orientation

Experiments have been run with the four-bladed, three-bladed, and perforated plate (intermediate-sized holes, thin plate) targets, with the drag flowmeter adapters on the top and bottom of the pipe and oriented horizontally. Graphs in Figs. 4.24 through 4.26 compare behavior of the intermediate-holed (thin) target in terms of R_2 when no flow-dispersing screens were used. With this target, the only differences among the three runs should be because of differences in average location of the center-of-force of the drag on the target, causing differences in effective length of the lever arm. (With the three-bladed target, the varying orientation causes varying proportions of target area in the upper and lower halves of the pipe, making data more difficult to interpret.) Comparing the three plots, it is clear that R_2 is generally highest for the lever arm entering the pipe from above (Fig. 4.24). R_2 is somewhat lower for adapter location on the side or on the bottom of the pipe (Figs. 4.25 and 4.26); there is, however, very little difference between the data from the latter two orientations. Although there is more scatter in the data for R_1 and R_3, they give a similar result for all targets tested.

In the air-water system, most momentum flux is due to the liquid phase at nearly all flow rates tested. If the mean center of force in

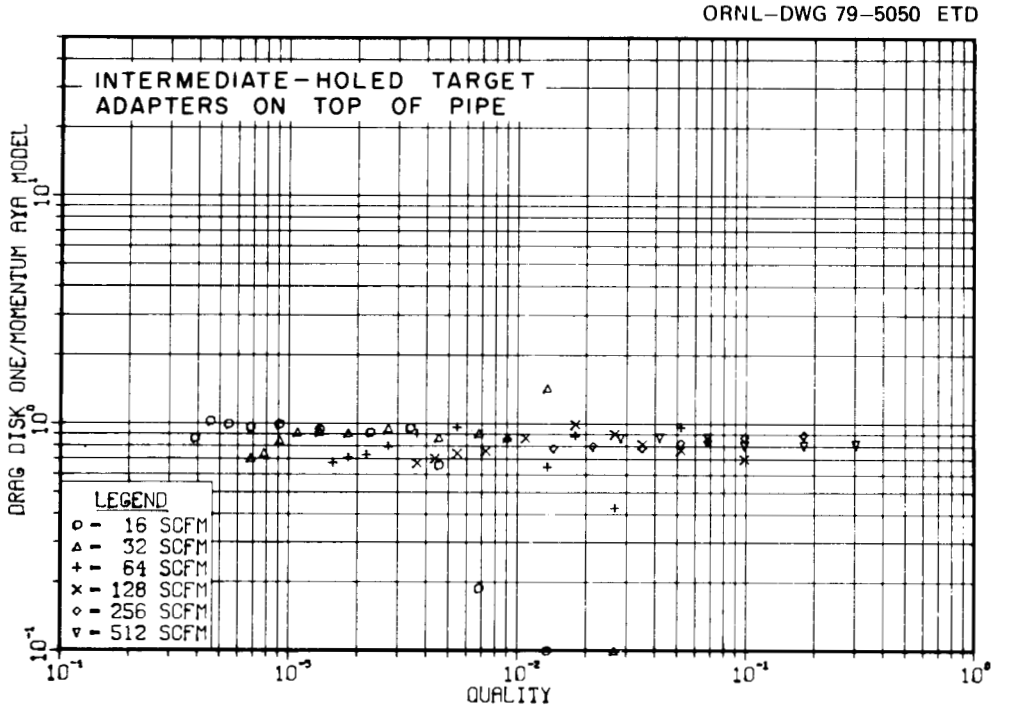

Fig. 4.24. R_2 vs quality, run 12, intermediate-holed target with adapters on top of pipe.

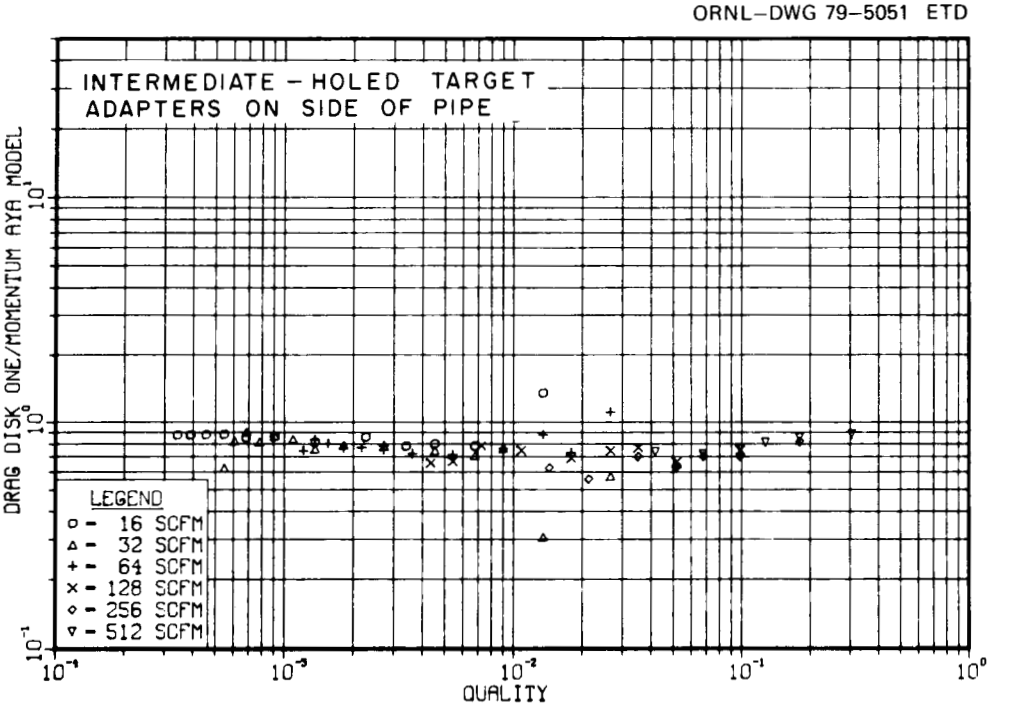

Fig. 4.25. R_2 vs quality, run 12, intermediate-holed target with adapters on side of pipe.

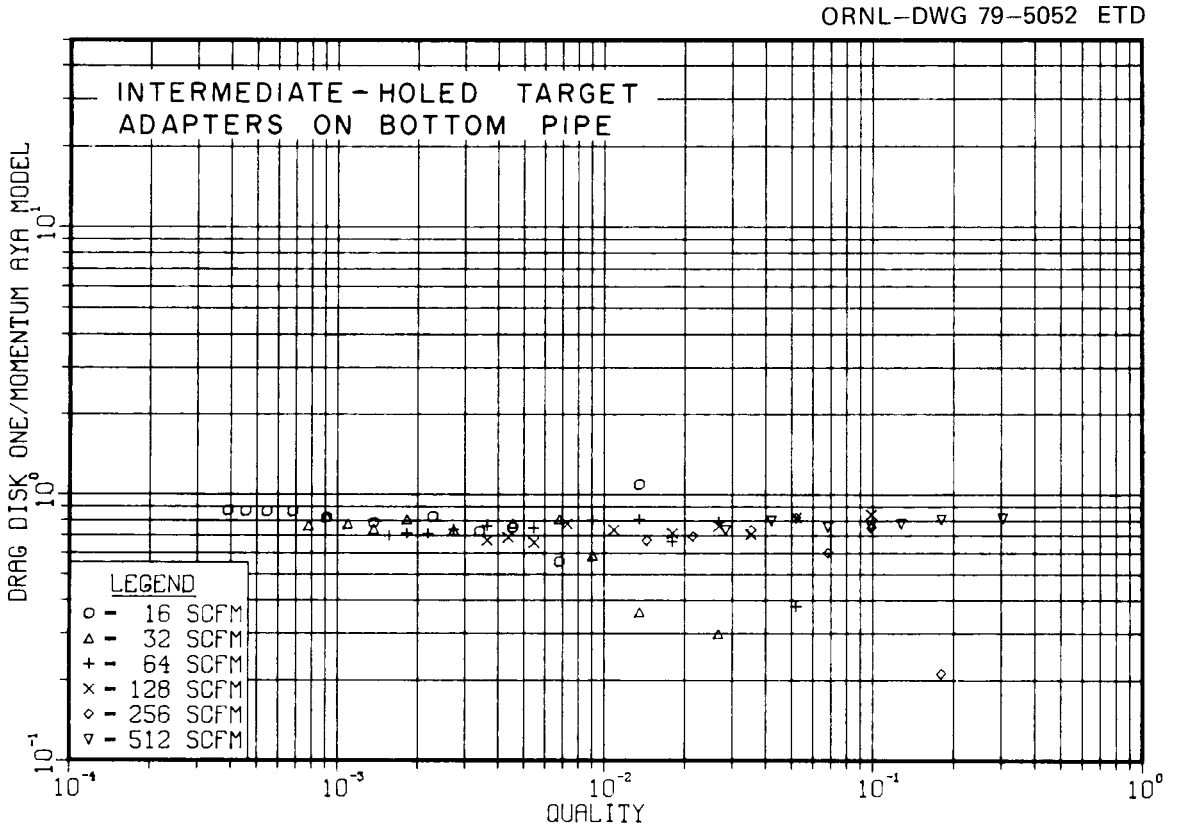

Fig. 4.26. R_2 vs quality, run 12, intermediate-holed target with adapters on bottom of pipe.

horizontal two-phase flow is below the pipe centerline, one would expect a drop in mean momentum flux in going from top- to side-adapter orientation, and a similar drop in going from side to bottom orientation. Preliminary analysis of data from advanced spool piece I indicates that the former decrease was observed but the latter was not. If the accuracy of the calculated results is high enough to make the results significant, we currently have no explanation for this behavior. During slug flow, rapidly moving slugs of water likely had a large proportion of their momentum flux in the top half of pipe; in these cases, the mean center-of-force might be very near the pipe centerline, and little effect of adapter orientation would be observed. In any case, the horizontal adapter orientation is recommended, even though the two-velocity momentum flux was underpredicted for most flow rates. Any variations in the center-of-force of the fluid would occur along an axis perpendicular

to the lever arm and would not affect the perpendicular distance between the strain gauge and the center-of-force.

4.4 Pressure Difference Measurements

4.4.1 Application of the Sheppard-Tong technique

A method of measuring two-phase mass flux by means of the pressure drop across flow-restricting screens is of much interest in the field of two-phase instrumentation. The technique used by Sheppard and Tong[20,21] to relate the pressure drop in the system to the mass flow rate was used in several of our two-phase flow experiments. Sheppard's pressure drop correlation to the mass flow rate is

$$\Delta P = C \left[\frac{G_L/A_p}{1 + (\bar{\rho}/\rho_\ell)} \right]^2 , \qquad (4.21)$$

in which G_L is the mass flow rate (lb_m/sec), $\bar{\rho}$ is the mean mixture density, and A_p is the cross-sectional area of the test section spool piece.

The pressure drop (in psid) measured across a 4-20 screen during run 6 is compared to the calculated mass flux (Fig. 4.27) in Eq. (4.21) using experimental data from the same test. The horizontal flow data agrees well with that of the Sheppard-Tong (Fig. 4.28) vertical downflow data, which indicates that the pressure drop across a screen might be a reasonable method of measuring the mass flow at qualities below ~1.5%. For the experiments that are performed at the ORNL air-water loop, this technique could become a better method of measurement if an improved means of measuring low pressure drop could be found. The amount of pressure drop within the system seems to be insignificant to the pressure transducer used in the advanced spool piece I, unless the drop is measured across a flow-restricting screen. Therefore, this technique is still primarily limited to the pressure drop across a flow-restricting or -dispersing screen.

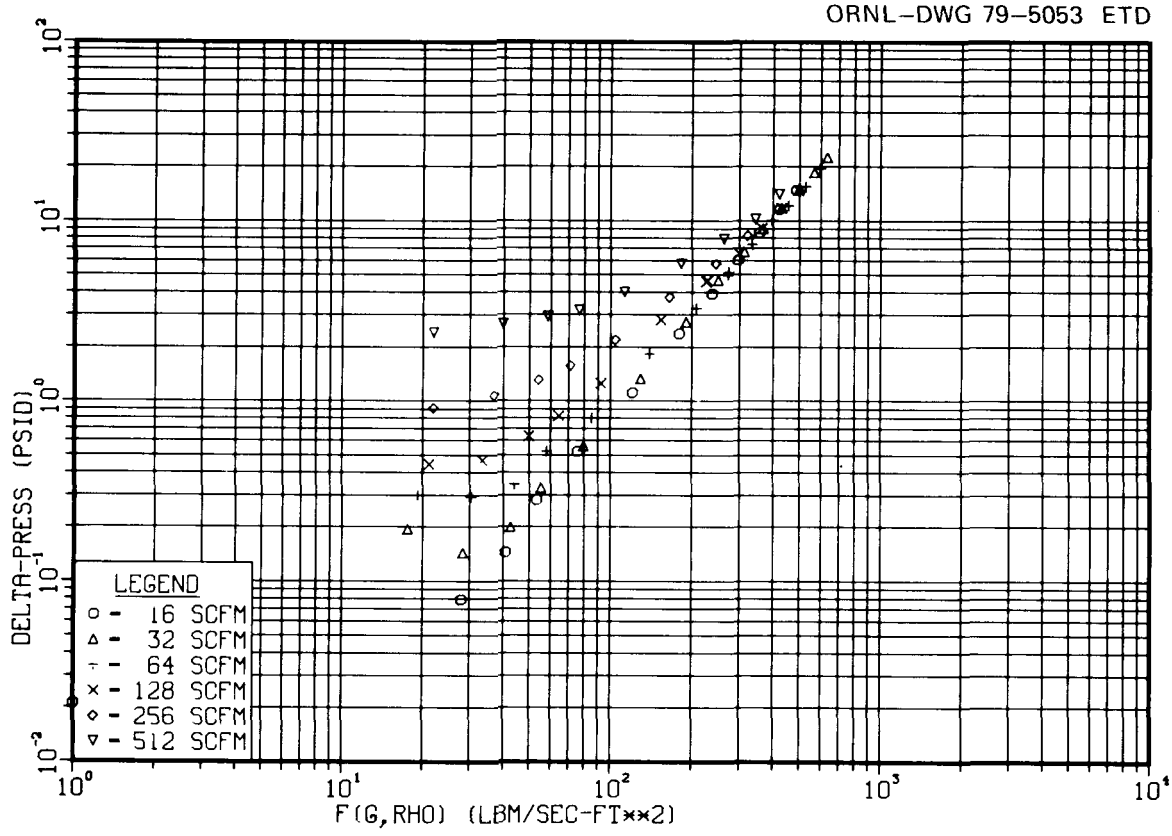

Fig. 4.27. Pressure drop of two-phase mixture flowing horizontally through one 4-20 screen with a 2.54-cm (1-in.) drag target plotted vs $F = G/(1 + \bar{\rho}/\rho_L)$.

4.4.2 Relation of ΔP to momentum flux

The pressure drop across a screen also may be related to the two-velocity momentum flux calculated using Eq. (4.14) in Fig. 4.29. There is a very linear relationship, with little scatter in all quality ranges. Figure 4.30 graphs the momentum flux ($lb_m/ft\text{-}sec^2$) measured by the drag flowmeter vs the pressure drop (psid) across a 4-20 screen. The drag flowmeter (the measured momentum flux) also behaves linearly with respect to the ΔP and the momentum flux, except that there is more scatter at the high momentum flux rates (Fig. 4.30). The curve in Fig. 4.30 begins to level off at 224 $kg/m\text{-}sec^2$ ($\sim$150 $lb_m/ft\text{-}sec^2$), which possibly could be explained by the effect of slow slug flow (discussed in Sect. 4.3.3).

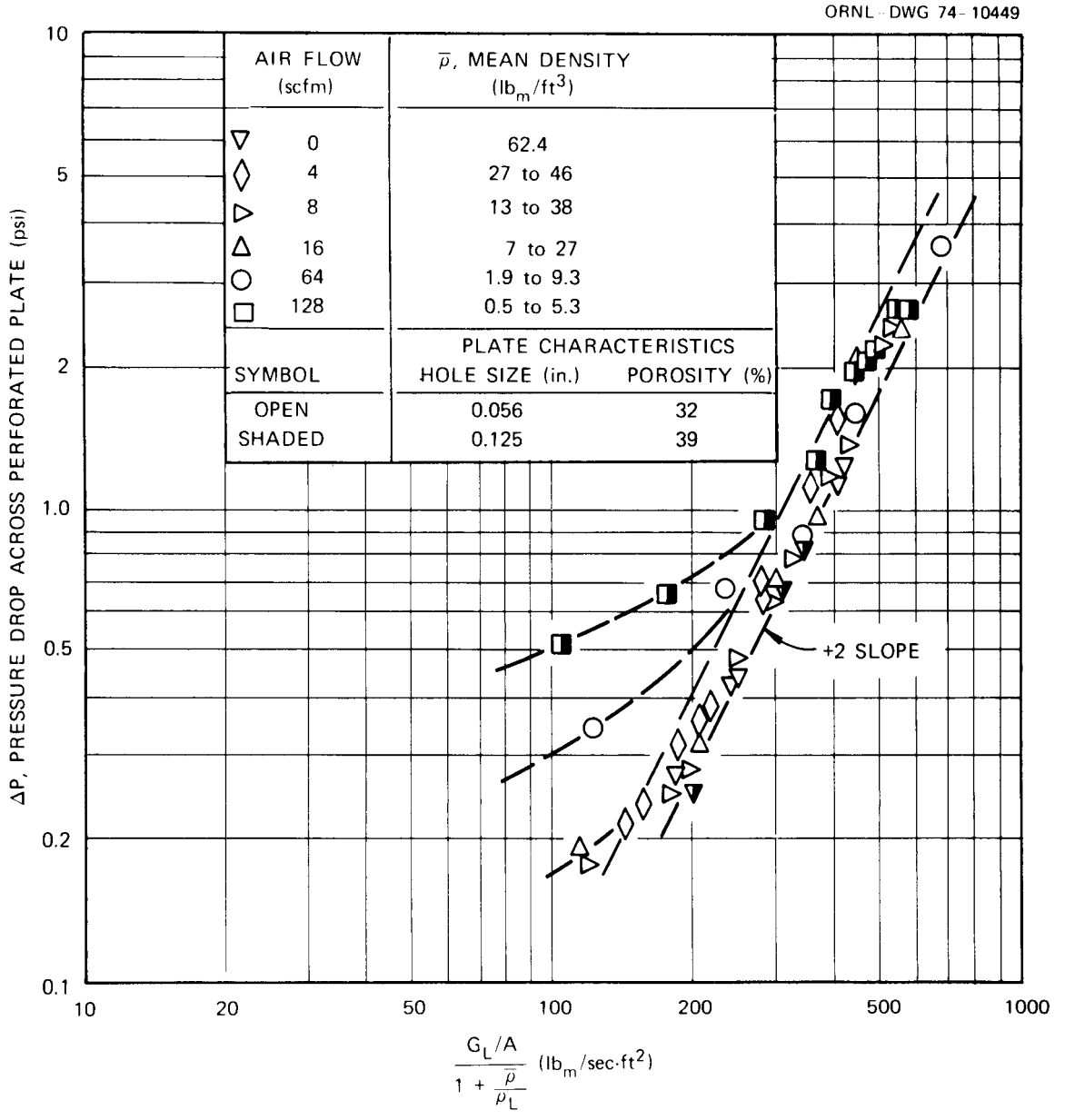

Fig. 4.28. Sheppard's pressure drop data[20] plotted vs $F = G_L/(1 + \bar{\rho}/\rho_L)$. Flow was vertically downward through a perforated plate.

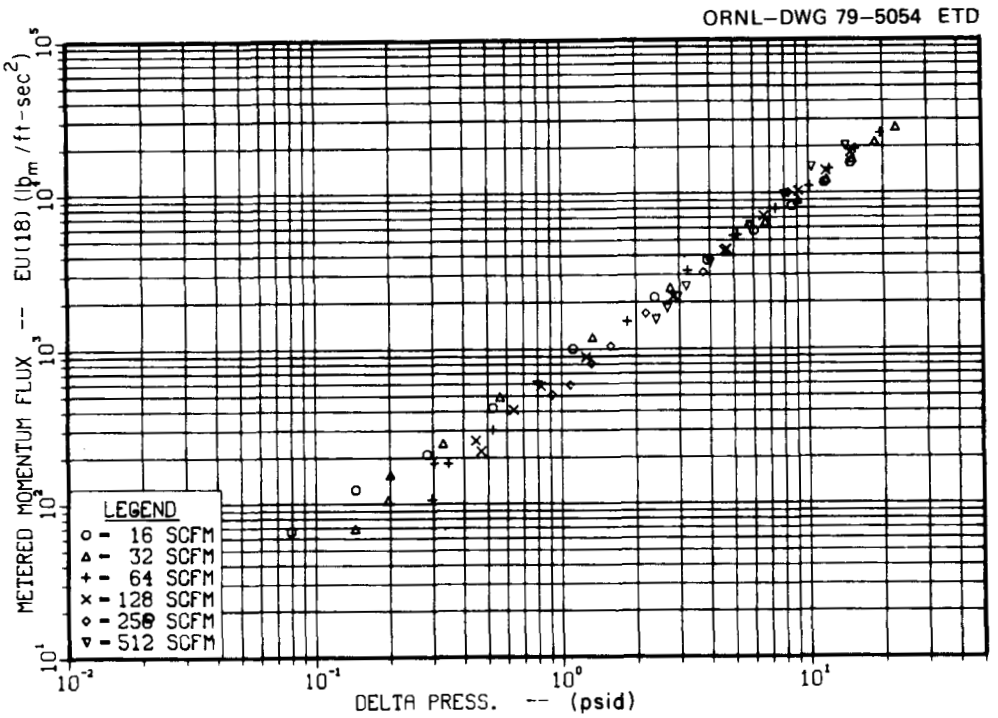

Fig. 4.29. Linear relationship exists between the pressure drop and the momentum flux calculated from the metered air and water inputs using a two-velocity model.

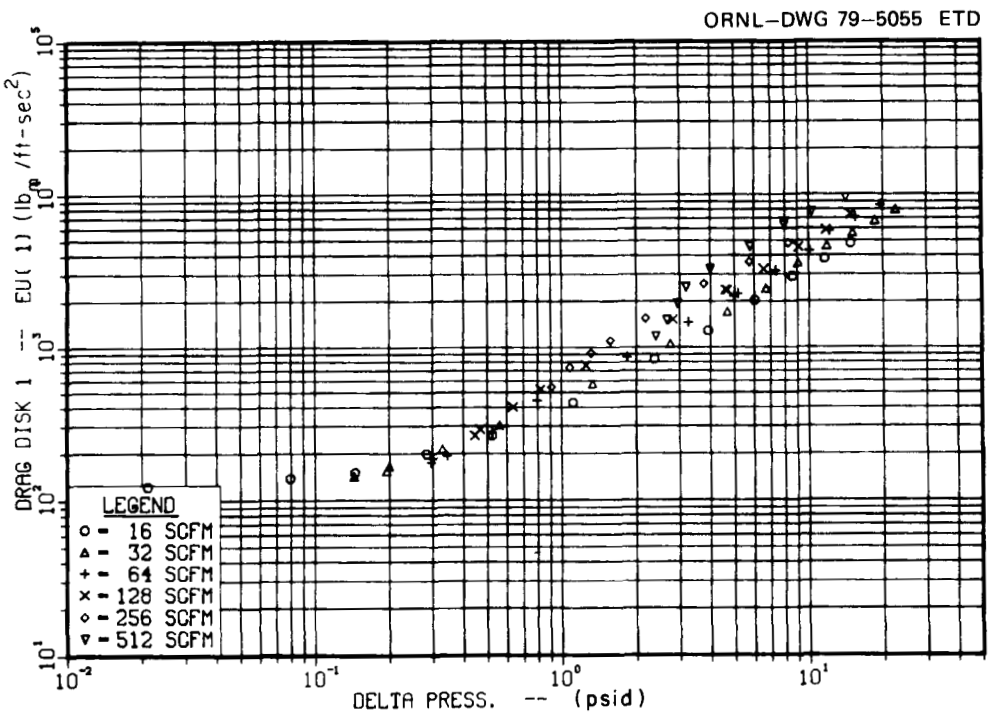

Fig. 4.30. Momentum flux calculated from the drag flowmeter is linear with respect to the pressure drop. More scatter in the data is apparent at higher momentum fluxes.

5. TWO-PHASE MASS FLOW MODELS

5.1 Homogeneous Models

Calculation of the mass flux from spool piece instrumentation can be accomplished by several methods, some of which assume a homogeneous mixture of the gas and liquid phases. Three methods which have been used to calculate the mass flux in the ORNL Air-Water Test Facility are

$$G_1 = (\bar{\rho}\, I_d)^{1/2} , \tag{5.1}$$

where $\bar{\rho}$ is the composite density and I_d is the momentum flux from the drag flowmeter;

$$G_2 = I_d/V_t , \tag{5.2}$$

which uses the turbine meter velocity V_t; and

$$G_3 = \bar{\rho}\, V_t . \tag{5.3}$$

These calculations, which assume homogeneous flow, could possibly lead to errors of interpreting the actual mass flux when compared with a mass flux that is calculated assuming a two-velocity flow profile. Evaluating G_1, G_2, and G_3 is interesting when the instrument behavior is postulated to be like that from two-velocity theory.[6]

To calculate the mass flux G_1 [(Eq. (5.1)], let the momentum flux and the composite density assume a two-velocity flow so that

$$G_2 = \{[\alpha\rho_g + (1 - \alpha)\rho_f][\alpha\rho_g V_g^2 + (1 - \alpha)\rho_f V_f]\}^{1/2} , \tag{5.4}$$

where α is the void fraction. For comparison, let the two-velocity mass flux calculation equal that of Eq. (4.19). For example, to estimate the effects of applying Eq. (5.1) to the test data from advanced spool piece I, the composite density from densitometer data and the single-phase

metered input rates were used to calculate α, V_f, and V_g for test 7. These values were then inserted into Eqs. (5.4) and (4.19). A plot of the ratio between Eqs. (5.4) and (4.19) shows a discrepancy of the ratio of the mass fluxes at qualities greater than 2% (Fig. 5.1). This gradual increase in the ratio is quite similar to calculations of the mass flux based on experimental data from the densitometer and drag flowmeter (Fig. 5.2). A two-velocity turbine meter calculation using the Aya[6] model was used in the mass flux calculations of Eqs. (5.2) and (5.3), which are also compared to Eq. (4.19) (Figs. 5.3 and 5.4). An increase also occurs in the ratio calculations based on Eqs. (5.2) and (5.3) at greater than 1% quality. A similar increase using the experimental data (Figs. 5.5 and 5.6) is also present. The increased ratio of modeled-to-actual mass fluxes at low air flow with low water flow which occurs for the actual experimental instruments (Figs. 5.2 and 5.5) was not predicted

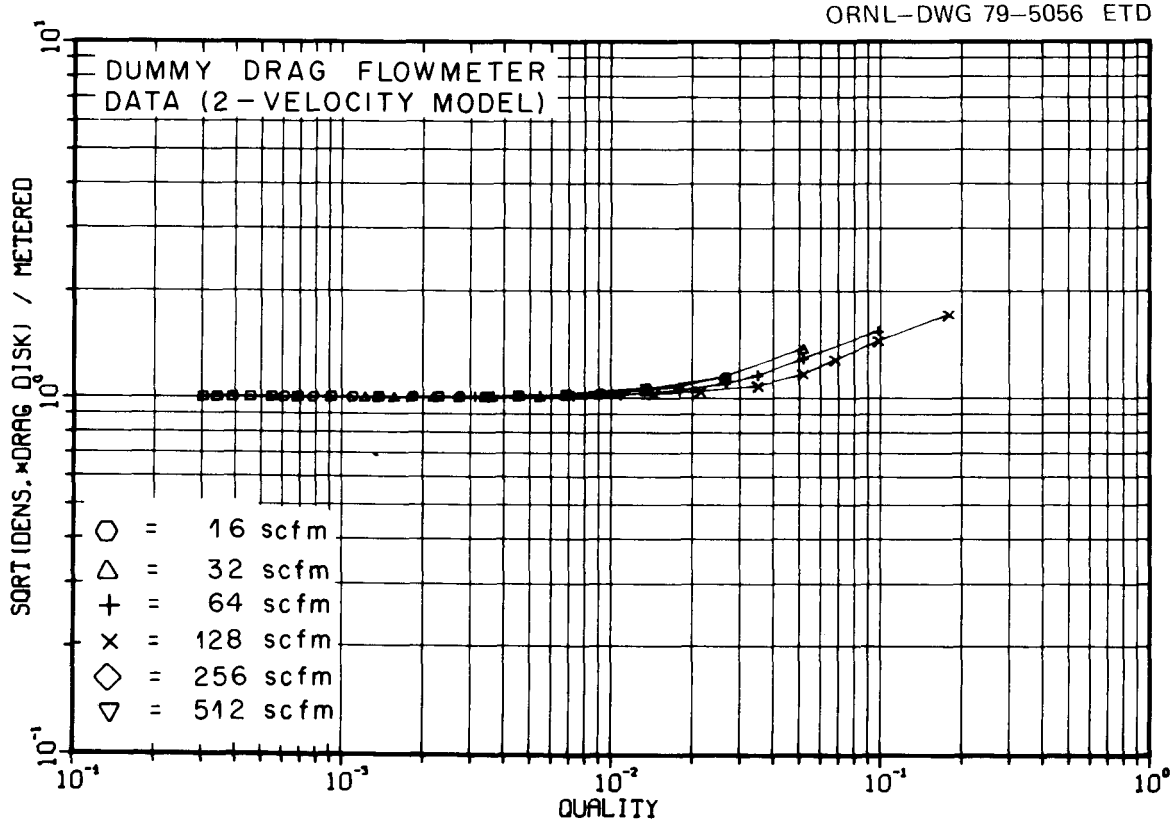

Fig. 5.1. Ratio of G_1 (calculated using a two-velocity assumption) to the actual mass flux, plotted vs quality.

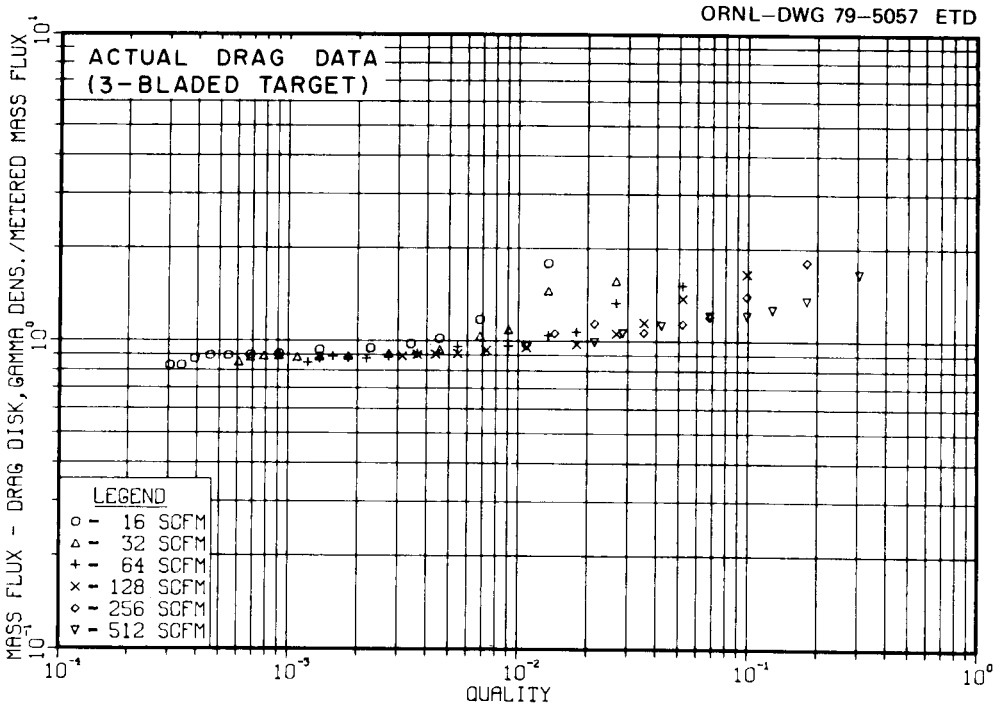

Fig. 5.2. Ratio of G_1 (calculated using densitometer and drag flowmeter data) to the actual mass flux, plotted vs quality.

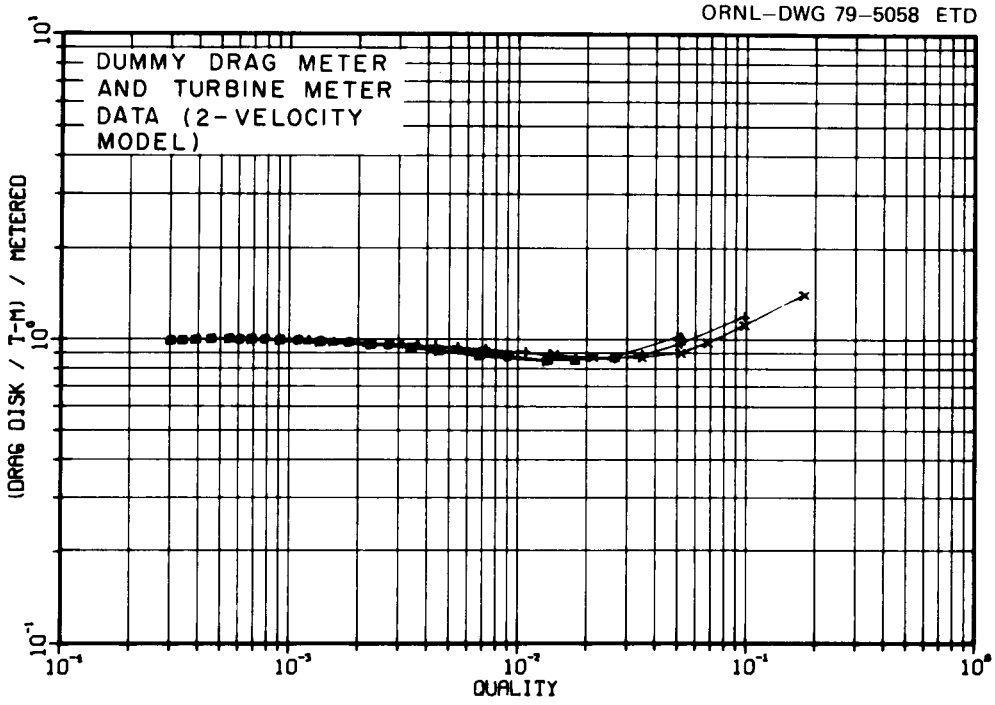

Fig. 5.3. Ratio of G_2 (calculated using a two-velocity assumption) to the actual mass flux, plotted vs quality.

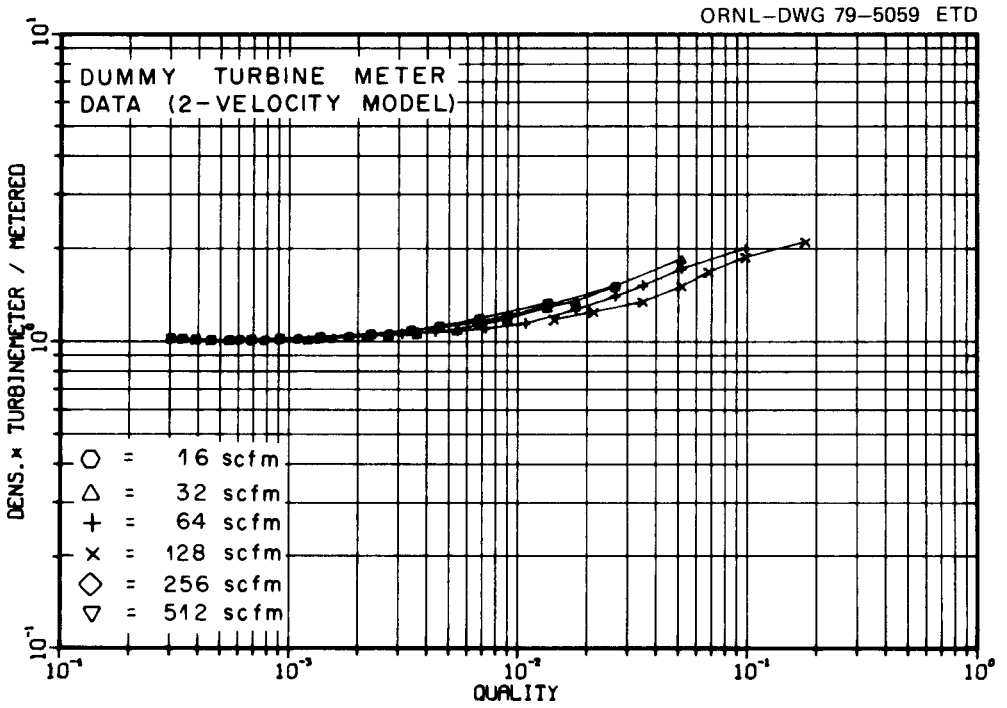

Fig. 5.4. Ratio of G_3 (calculated using a two-velocity assumption) to the actual mass flux, plotted vs quality.

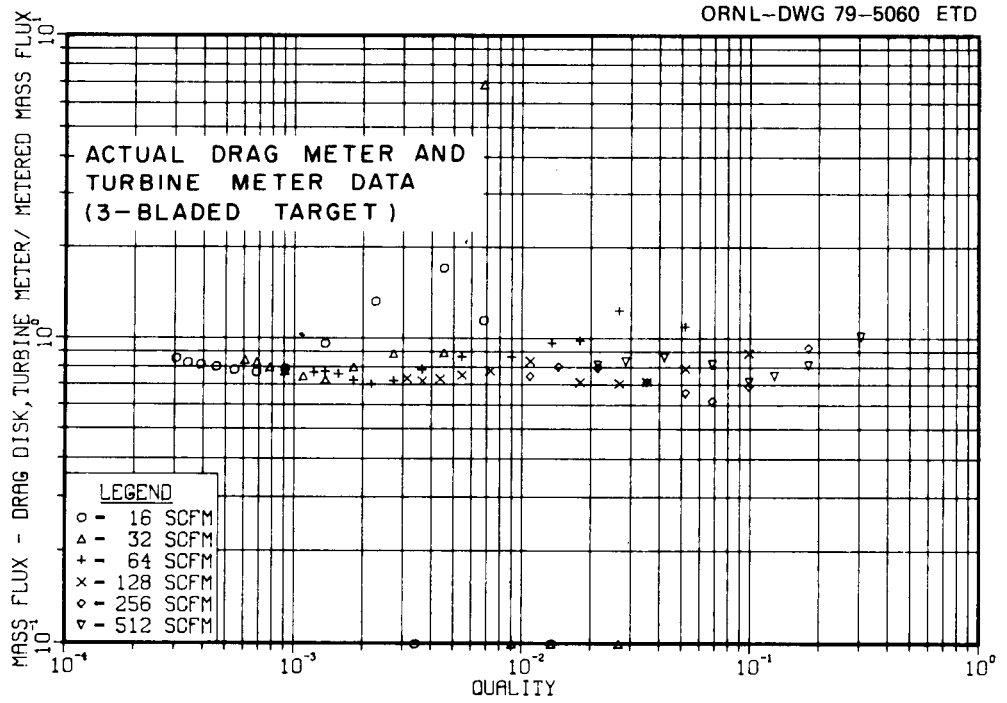

Fig. 5.5. Ratio of G_2 (calculated using turbine and drag flowmeter data) to the actual mass flux, plotted vs quality.

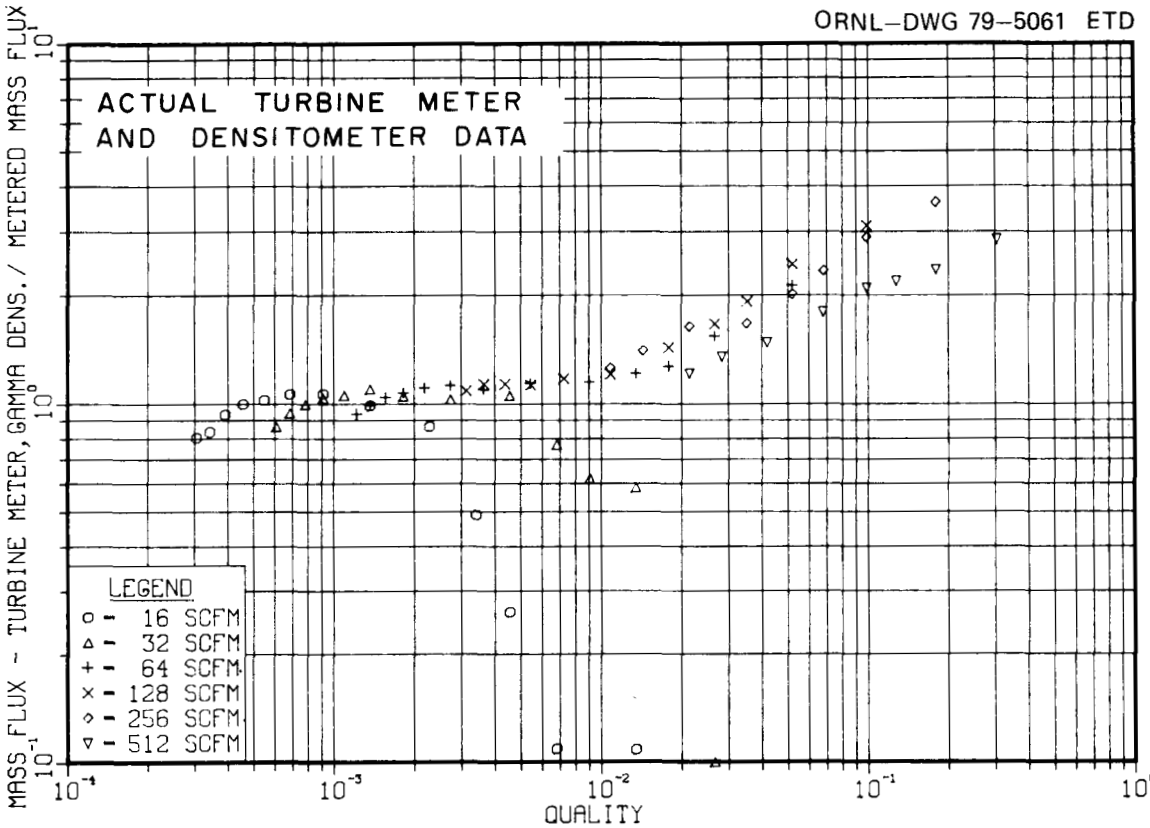

Fig. 5.6. Ratio of G_3 (calculated using densitometer and turbine data) to the actual mass flux, plotted vs quality.

in the two-velocity calculations (Figs. 5.1 and 5.3) because the calculation of V_f and V_g is incorrect in slow slug flow. The predominance of the experimental data below unity at low qualities was not predicted because no decrease in the two-phase drag coefficient was assumed. [As noted earlier (Sect. 4.2.2), the Rouhani model simulates turbine meter performance better than does the Aya model at higher qualities. Substitution of the Rouhani turbine formula into Eq. (5.2) may give a more consistent ratio, like that found for R_3 in the discussion of drag body behavior.]

This increase of the mass flux ratio at high qualities is present in our tests that use different drag targets and different testing conditions.

This indicates that the drag flowmeter and turbine meter are not necessarily performing inconsistently but that the homogeneous models

used to calculate the mass flux from their measurements are more unrealistic than are the two-velocity models.

5.2 Aya Model

The model proposed by Aya[6] has been used extensively to calculate two-phase mass flow rates from the readings of a turbine meter (V_t), drag flowmeter (I_d), and densitometer (ρ_a). Application of the model to data from advanced spool piece I has revealed that a direct solution for mass flux and related quantities is sometimes not possible when using the mathematical form proposed by Aya. For example, the equation for liquid velocity V_f is

$$V_f = \begin{cases} a + b , & S \leq \overline{C}_d \sqrt{Y/\overline{C}_t} \\ a - b , & S > \overline{C}_d \sqrt{Y/\overline{C}_t} \end{cases} , \tag{5.5}$$

where

$$a = \sqrt{\frac{\overline{C}_t}{Y}} \left(\frac{1 + \sqrt{\overline{C}_t\, Y}}{\overline{C}_d + \overline{C}_t} \right) V_t ,$$

$$b = \frac{1}{\overline{C}_d + \overline{C}_t} \left[(\overline{C}_d + \overline{C}_t) \left(\frac{\rho_f - \rho_g}{\rho_a - \rho_g} \right) \frac{I_d}{\rho_f C_{dg}} - \frac{\overline{C}_d}{Y} \left(1 + \sqrt{\overline{C}_t\, Y} \right)^2 V_t^2 \right]^{1/2} ,$$

$$Y = \rho_f/\rho_g \left(\frac{\rho_a - \rho_g}{\rho_f - \rho_a} \right) ,$$

and

$$\overline{C}_d = C_{df}/C_{dq} ,$$

$$\overline{C}_t = C_{tf}/C_{tg} .$$

[Equation (5.5) corresponds to Eq. (18) in Ref. 6.] Frequently, the assumption is made that $\overline{C}_d = \overline{C}_t = 1$. For this study, that seems justified because of single-phase air and water calibration results from various drag targets and because of the results obtained with the Aya turbine model described in Sect. 4.2.2.

Section 4.3.4 notes that, for many of the two-phase flow rates studied, especially at qualities below ∿2%, the full-flow drag targets seem to have two-phase drag coefficients less than the single-phase values. Thus, quite often, the indicated momentum fluxes I_d have been lower than might otherwise be expected.

In addition, the turbine model study described in Sect. 4.2.2 suggests that, at the highest qualities tested, the turbine velocities are significantly higher than predicted using the Aya turbine assumption. Clearly, either of these factors can lead to calculation of a negative value for the term in square brackets in Eq. (5.5); in such cases, the value of b would be undefined, causing the failure of the model. For a typical run, the use of the measured values of I_d, V_T, and ρ_a led to such failures for most points taken at 60, 121, and 242 liters/sec (128, 256, and 512 scfm). In subsequent analysis, we have taken the approach of setting b to zero when the negative difference was calculated to occur.

In application of the Aya model, evaluating the slip ratio S is necessary using the value of V_f from Eq. (5.5),

$$S^2 = \frac{(\rho_f - \rho_g)(I_d/C_{dg}) - (\rho_a - \rho_g)\,\rho_f\,\overline{C}_d\,V_f^2}{(\rho_f - \rho_a)\,\rho_g\,V_f^2}\,, \tag{5.6}$$

where Eq. (5.6) is Eq. (7) in Ref. 6. In the air-water system, ρ_g is often insignificant compared to ρ_f and ρ_a; C_{dg} and $\overline{C}_d$ are again assumed to be unity. The factors I_d and $\rho_a V_f^2$ therefore are both multiplied by ρ_f. In application of the model to the data, we have found that, for the highest qualities, V_f from Eq. (5.5) tends to underestimate the V_f indicated by the metered liquid volumetric input rate and the void fraction. In some cases, the numerator of Eq. (5.6) has been negative,

causing the slip ratio and the mass flux to be undefined. For run 19 (three-bladed drag targets, one 4-20 screen), this type of model failure occurred for the data taken at 0.6 and 1.3 liters/sec (10 and 20 gpm) water flow rates, with air flow rates of 60 liters/sec (128 scfm) and higher.

It was noted previously that, for low air and water flow rates, the turbine meter signal may be zero. The turbine rotor is in fact spinning, but there is an effective speed threshold below which the electronics output is zero. Checking the effect of this on application of the Aya model is interesting. From Eq. (5.5) for V_f, term a will be identically zero if $V_t = 0$. The second term in square brackets in the equation for b will also be zero. Neglecting ρ_g and ρ_a, we have then

$$V_f = \sqrt{\frac{I_d}{2\rho_a}} \, . \tag{5.7}$$

Substituting this into Eq. (5.6) for S^2, we get

$$S^2 = \frac{\rho_f}{\rho_g} \, \frac{\rho_a}{\rho_f - \rho_a} \, . \tag{5.8}$$

Surprisingly, when $V_T \to 0$ and when ρ_g is small with respect to ρ_a, the slip ratio depends only on the phase densities and the void fraction. The model thus tends to ignore intermittent or zero turbine readings.

In the analysis of data from run 19, the time-averaged turbine, densitometer, and drag flowmeter readings were used in the Aya model. In this case, the calculated value was the result of applying the model calculations to instrument readings averaged over each scan (see Sect. 3). The calculated ratio of mass flux from the Aya model to the "actual" mass flux based on single-phase metered inputs appears in Fig. 5.7. The six points where the model failed because S^2 was negative are not plotted; these points would have been for qualities above 5%. At times when the mean turbine velocity V_t was very low but positive, the model still calculated reasonable mass fluxes.

To better understand the Aya model performance for this run, a study was made to evaluate the importance of the input momentum flux I_d on the

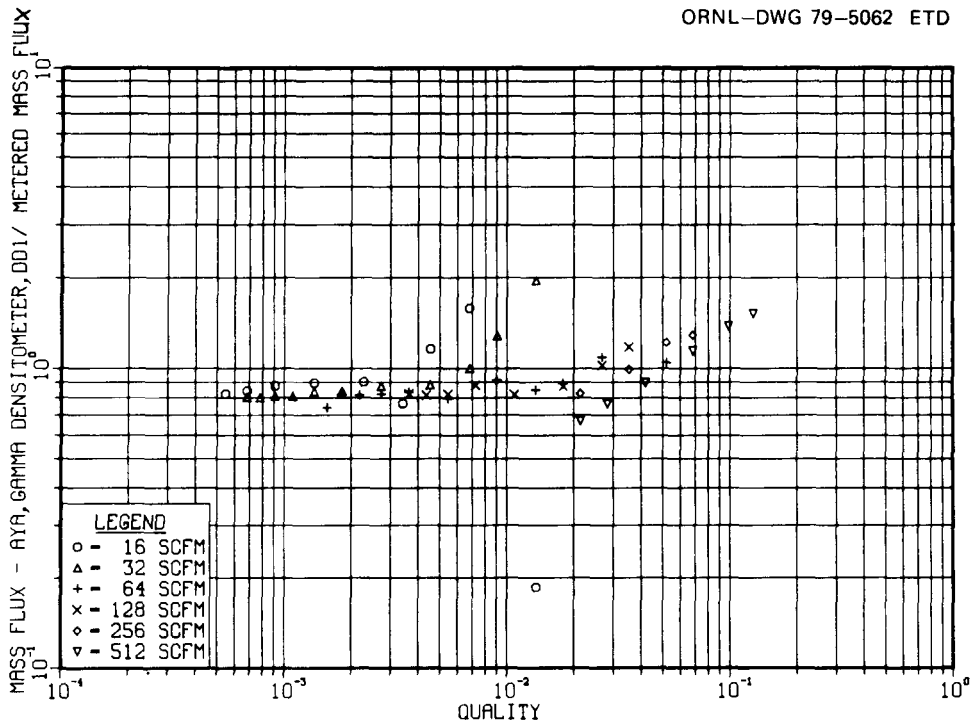

Fig. 5.7. Ratio of mass flux calculated using the Aya model to the actual mass flux, plotted vs quality, run 19. Points where model failed because of undefined slip ratio were not plotted.

accuracy of the calculated mass flux. Instead of the reduced drag flowmeter reading, the two-velocity momentum flux, defined by Eq. (4.13), was input to the model, but the turbine velocity V_t and the apparent density ρ_a from the densitometer data were retained. Results from the calculation (Fig. 5.8) show that most of the error in Aya mass flux arises from error in the drag flowmeter reading; a similar result was obtained by Estrada[15] using vertical downflow data from the ORNL air-water loop. At qualities below ∿1%, virtually perfect agreement with the metered inputs was obtained. Between 1 and 10% quality, a small but increasing amount of scatter occurred in the data. Again, at 10% quality, the model failed because S^2 was negative. The momentum flux I_d calculated from the drag flowmeter output using single-phase calibration data does not likely correspond to the two-velocity momentum flux in the manner used for data reduction. The ratio of I_d from the drag flowmeter to the two-velocity momentum fluxes in run 19 is shown in Fig. 5.9; note the similarity between Figs. 5.7 and 5.9.

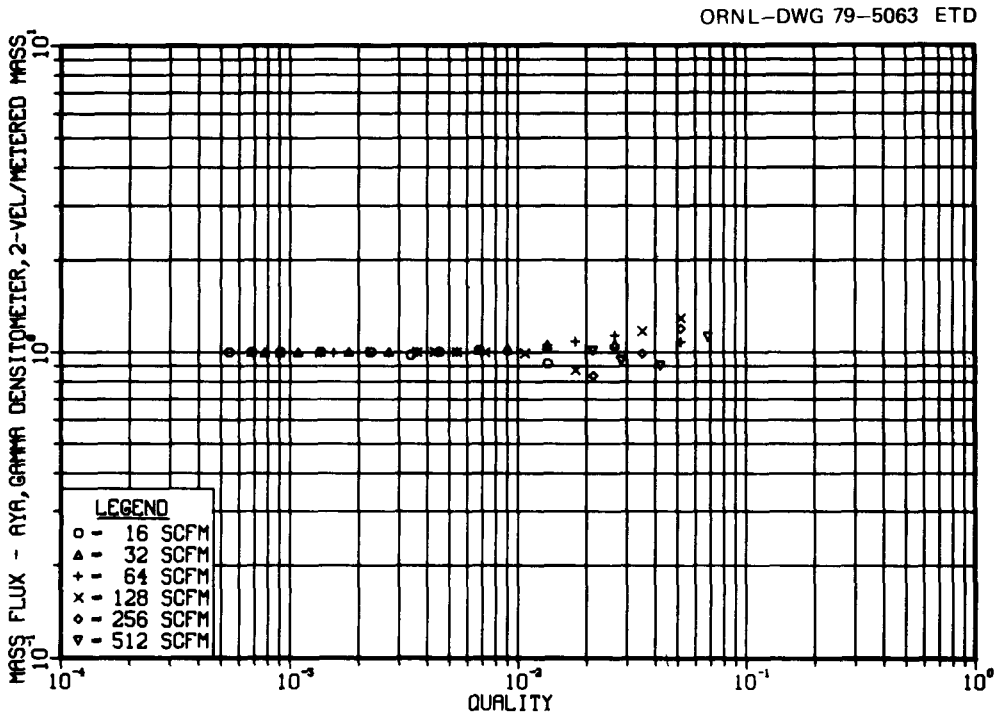

Fig. 5.8. Ratio of mass flux calculated using the Aya model to the actual mass flux, plotted vs quality, run 19. Calculated momentum flux [Eq. (4.14)], has been used instead of the drag flowmeter reading; actual turbine and densitometer data were used.

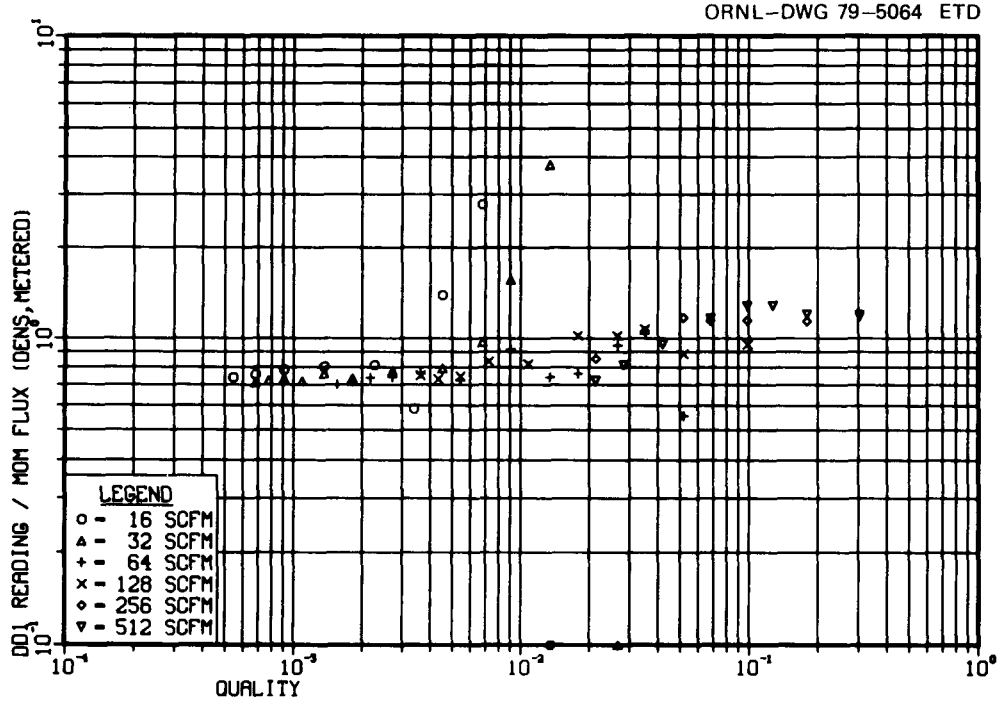

Fig. 5.9. R_1 vs quality, run 19.

6. SUMMARY AND CONCLUSIONS

Testing of advanced spool piece I in a horizontal orientation in the ORNL air-water loop has been completed. Two-phase experiments with a number of drag targets, with three spool piece azimuthal orientations, and with and without flow-dispersing screens have been performed.

Preliminary analysis of experimental data from the horizontal tests has been completed. A major improvement has been made in the data reduction computer code, allowing evaluations of models and instrument performance in a manner like that used in blowdown analysis.

When full-flow drag targets were used in advanced spool piece I, considerable disturbance of the flow regime occurred at the plane of the densitometer. The calculated composite densities were most seriously affected at the lowest void fractions when use of large targets caused underestimates of the density by annular and stratified models.

Analysis of turbine meter output has revealed that the turbine meter electronics developed recently by the ORNL Instrumentation and Controls Division are superior to the electronics supplied by the turbine manufacturer. The new electronics have much better time response and allow detection of much lower rotor speeds than do the old electronics. A study was made in which mean phase velocities (based on metered inputs and densitometer data) were substituted into expressions for the turbine velocity postulated by Aya, Rouhani, and the volumetric model. Comparisons between the turbine speeds predicted by the models and mean turbine speeds recorded in horizontal flow revealed that the Aya and Rouhani models perform well, with the Rouhani model doing slightly better.

Nine drag target designs (Fig. 4.15 and Table 4.1) were tested with the flowmeter lever arms entering from the top of the pipe. A momentum flux was calculated using single-phase calibration factors and drag transducer output. This was compared to a two-velocity momentum flux based on either turbine meter or density data and metered inputs to the loop. The mass flux calculation $G = I_D/V_T$ was also used in evaluation of target behavior. Results indicate that the three-bladed, four-bladed, and perforated plate targets with intermediate-sized holes (Table 4.1) performed somewhat better than the other targets tested. Except for flow

rates with low air and water inputs, the average two-phase drag coefficients estimated using the above methods were significantly less (20 to 30%) than the single-phase coefficients. Flow-dispersing screens were found to have a negligible effect on the full-flow drag targets in horizontal flow. The drag flowmeter downstream of the turbine meter performed reasonably well in advanced spool piece I over most of the flow rates used. Observed effects of drag lever arm orientation were inconsistent; an apparent decrease in lever arm length, which was noted when the lever arms were rotated from top entry to horizontal, was not seen when a further rotation was made beneath the pipe.

Pressure-difference measurements taken across a flow-dispersing screen during two-phase flow were used in the mass flux model proposed by Sheppard. The agreement with measured values was good below qualities of 1.15%. However, the pressure-difference measurements were found to be in almost direct proportion to the calculated two-velocity momentum flux over nearly all flow rates.

Calculations were made in which the homogeneous mass flux models $G = \overline{\rho} V_t$ and $G = (\overline{\rho} I_d)^{1/2}$ were applied using the substitutions

$$\overline{\rho} = \rho_{composite} ,$$

$$V_t = V_{t_{Aya}} (V_f, V_g) ,$$

$$I_d = (1 - \alpha)\rho_f V_f^2 + \alpha \rho_g V_g^2 ,$$

$$V_f = \frac{Q_f}{A(1 - \alpha)} ,$$

and

$$V_g = \frac{Q_g}{A\alpha} .$$

The calculated mass fluxes agreed well with those calculated using actual

instrument responses for V_t and I_d. At qualities above ~2%, neither of the methods agree well with the actual fluxes. This indicates that, at least for horizontal flow, the air-water two-phase flow behavior is much better approximated by two-velocity models than by homogeneous models, especially at higher qualities.

The Aya model did not give significantly better results than the homogeneous models used. Part of the errors may be caused by underestimates of two-phase momentum fluxes by the drag flowmeter. At some flow rates, this caused failure of the Aya model altogether. The model given by $G_3 = I_d/V_T$ was found to yield very consistent mass flux calculations with respect to the actual values. (G_3 conforms to a two-velocity assumption, if the Rouhani-Estrada turbine model is used.) Only when the turbine signal output was zero or intermittent did that model fail. Because of the low two-phase drag coefficients for most targets, G_3 underestimated the actual mass flux by 10 to 30%, but that behavior was consistent over the entire range of flow rates used.

REFERENCES

1. J. D. Sheppard et al., *Advanced Two-Phase Instrumentation Program Quarterly Progress Report for January–March 1977*, ORNL/NUREG/TM-119.

2. J. D. Mandhane et al., "A Flow Pattern Map for Gas-Liquid Flow in Horizontal Pipes," *Int. J. Multiphase Flow* 1, 537–53 (1974).

3. K. G. Turnage et al., *Advanced Two-Phase Instrumentation Program Quarterly Progress Report for April–June 1978*, ORNL/NUREG/TM-279.

4. R. A. Hedrick et al., *PWR Blowdown Heat Transfer Separate-Effects Program Data Evaluation Report — System Response for Thermal Hydraulic Test Facility Test Series 100*, ORNL/NUREG-19 (November 1977).

5. S. Z. Rouhani, "Application of the Turbine Type Flowmeters in the Measurements of Steam Quality and Void," *Symposium on In-Core Instrumentation, Oslo, Norway, June 1974*.

6. Izuo Aya, *A Model to Calculate Mass Flow Rate and Other Quantities of Two-Phase Flow in a Pipe with a Densitometer, a Drag Disk, and a Turbine Meter*, ORNL/TM-4759 (November 1975).

7. S. Banerjee, "A Review of Mass Velocity Measurements in Two-Phase Flows," Presented at course on two-phase flow measurements, Fluid Dynamic Institute, Dartmouth College, Hanover, N.H., August 1978.

8. P. S. Kamath and R. T. Lahey, Jr., "A Turbine Meter Evaluation Model for Two-Phase Transients (TEMPT)," Topical Report RPI, NES-459, prepared for EG&G Idaho by Department of Nuclear Engineering (October 1977).

9. D. G. Thomas et al., *Blowdown Heat Transfer Separate-Effects Program Quarterly Progress Report for July–September 1976*, ORNL/NUREG/TM-61, Sect. 2.3.

10. A. H. Hsia et al., *Rod Bundle Test Facility Instrumentation Description, Calibration, and Uncertainty Analysis, PWR Blowdown Heat Transfer Project*, EPRI/NP-112, pp. 4-109–4-140 (August 1977).

11. J. R. Fincke, *Development of the LOFT Prototype Drag Screen–Air-Water Testing*, TREE-NUREG-1198 (May 1978).

12. J. R. Fincke, *Development of the LOFT Prototype Drag Screen–Transient Steam-Water Testing*, TREE-NUREG-1241 (July 1978).

13. G. B. Andeen and P. Griffith, "Momentum Flux in Two-Phase Flow," *J. Heat Transfer*, pp. 211–22 (May 1968).

14. EG&G Idaho, Inc., *Quarterly Technical Progress Report on Water Reactor Safety Programs Sponsored by the Nuclear Regulatory Commission's Division of Reactor Safety Research, January–March 1978*, TREE-NUREG-1218, Sect. I.2 (April 1978).

15. MPR Associates, Inc., *Interpreting Two-Phase Flow Measurements*, MPR-511 (May 1976).

16. S. F. Hoerner, *Fluid Dynamic Drag*, 2nd ed., published by the author, pp. 3.14–3.16, 10.7–10.10, 1965.

17. K. G. Turnage et al., *Advanced Two-Phase Instrumentation Program Quarterly Progress Report for January–March 1978*, ORNL/NUREG/TM-250.

18. J. D. Sheppard, *Quarterly Progress Report on Reactor Safety Programs for October–December 1974*, ORNL/TM-1805, pp. 66–77.

19. P. A. Jallouk and J. E. Hardy, *Advanced Two-Phase Instrumentation Program Quarterly Progress Report for October–December 1977*, ORNL/NUREG/TM-227, pp. 1–19.

20. J. D. Sheppard et al., *Quarterly Progress Report on Reactor Safety Programs for July–September 1974*, ORNL/TM-4729, pp. 43–46.

21. J. D. Sheppard and L. S. Tong, Apparatus for Monitoring Two-Phase Flow, U.S. Patent 4009614, March 1977.

NUREG/CR-0686
ORNL/NUREG/TM-309
Dist. Category R2

Internal Distribution

1. M. Bender
2. S. B. Cliff
3. S. K. Combs
4. W. B. Cottrell
5. W. G. Craddick
6. C. E. Davis
7. I. T. Dudley
8. B. G. Eads
9. H. L. Falkenberry
10. R. C. Hagar
11. J. E. Hardy
12. M. Herskovitz
13. H. W. Hoffman
14. W. H. Leavell
15. R. N. McGill
16. F. R. Mynatt
17. H. Postma
18. J. L. Rich
19. M. J. Roberts
20. D. G. Thomas
21. H. E. Trammell
22. D. B. Trauger
23. K. G. Turnage
24. J. D. White
25. M. D. White
26. ORNL Patent Office
27-28. Central Research Library
29. Document Reference Section
30-32. Laboratory Records Department
33. Laboratory Records (RC)

External Distribution

34-41. Director, Division of Reactor Safety Research, Nuclear Regulatory Commission, Washington, D.C. 20555
42. Director, Reactor Division, DOE, ORO
43. Office of Assistant Manager, Energy Research and Development, DOE-ORO
44-48. Director, Reactor Safety Research Coordination Office, DOE, Washington, D.C. 20555
49-50. DOE-TIC, P.O. Box 62, Oak Ridge, Tenn. 37830
51-350. Given distribution as shown under category R2 (NTIS-25)

☆U.S. GOVERNMENT PRINTING OFFICE: 1979-640-079-38